Acta Pharmaceutica Sinica B 2024;14(12):5321−5340

Chinese Pharmaceutical Association
Institute of Materia Medica, Chinese Academy of Medical Sciences

Acta Pharmaceutica Sinica B

www.elsevier.com/locate/apsb
www.sciencedirect.com

ORIGINAL ARTICLE

Avenanthramide A potentiates Bim-mediated antineoplastic properties of 5-fluorouracil *via* targeting KDM4C/*MIR17HG*/GSK-3β negative feedback loop in colorectal cancer

Rong Fu [a,b], Zhangfeng Dou [e], Ning Li [e], Xueyuan Fan [d], Sajid Amin [f], Jinqi Zhang [b], Yuqing Wang [b], Zongwei Li [c,*], Zhuoyu Li [b,*], Peng Yang [b,*]

[a]*School of Basic Medical Sciences, Shanxi Medical University, Taiyuan 030001, China*
[b]*Institute of Biotechnology, Key Laboratory of Chemical Biology and Molecular Engineering of National Ministry of Education, Shanxi University, Taiyuan 030006, China*
[c]*School of Life Science, Anhui Medical University, Hefei 230032, China*
[d]*School of Life Science, Shanxi University, Taiyuan 030006, China*
[e]*Department of Gastroenterology, First Hospital of Shanxi Medical University, Taiyuan 030001, China*
[f]*Department of Precision Medicine, University of Campania Luigi Vanvitelli, Naples 80138, Italy*

Received 20 February 2024; received in revised form 24 May 2024; accepted 10 July 2024

KEY WORDS

Avenanthramide A;
5-Fluorouracil;
KDM4C;
Colorectal cancer;
MIR17HG

Abstract Chemoresistance to 5-fluorouracil (5-FU) is a significant challenge in treating colorectal cancer (CRC). Novel combined regimens to thwart chemoresistance are therefore urgently needed. Herein, we demonstrated that the combination of Avenanthramide A (AVN A) and 5-FU has significant therapeutic advantages against CRC. Mechanistically, AVN A directly binds to the S198 site of the histone lysine demethylase KDM4C to promote its degradation, which subsequently fosters H3K9me3 occupancy on the *MIR17HG* promoter to block its transcription and derepress Bim expression. AVN A enhanced the therapeutic efficacy of 5-FU *via* impairing the KDM4C/*MIR17HG*/GSK-3β negative feedback loop. Importantly, the clinical correlation of the KDM4C/*MIR17HG*/Bim signaling axis with 5-FU response was validated in the refractory CRC patients. We provide evidence for the enhanced effectiveness of 5-FU when combined with AVN A in chemoresistant xenografts, CRC organoids, and $Apc^{Min/+}$ mouse model. Additionally, AVN A mitigated the systemic adverse effects of 5-FU. Overall, our findings

*Corresponding authors.
E-mail addresses: lizongwei@ahmu.edu.cn (Zongwei Li), lzy@sxu.edu.cn (Zhuoyu Li), peng114011@sxu.edu.cn (Peng Yang).
Peer review under the responsibility of Chinese Pharmaceutical Association and Institute of Materia Medica, Chinese Academy of Medical Sciences.

https://doi.org/10.1016/j.apsb.2024.07.018

demonstrate that combinatorial therapy with AVN A and 5-FU represents an appealing opportunity and highlights KDM4C/*MIR17HG*/GSK-3β negative feedback loop which confers therapeutically exploitable vulnerability to chemo-refractory CRC patients.

1. Introduction

Colorectal cancer (CRC) is one of the most prevalent cancer types globally[1,2]. 5-Fluorouracil (5-FU) remains the first-line therapy for advanced-stage CRC patients[3]. Despite the fact that 5-FU-based chemotherapies show a considerable initial response in CRC patients, the overall clinical outcome of CRC remains drastically poor, which is primarily attributed to an inevitable relapse with chemotherapy-resistant characteristics of cancer[4]. In addition, 5-FU also causes systemic adverse effects including gastrointestinal toxicity, immunosuppression, and liver and kidney damage, which confine its use in clinical practices. The mechanisms underlying 5-FU resistance are complex, including drug metabolism, imbalance of apoptosis-related proteins, miRNA dysregulation, and abnormal epigenetic regulation[5,6]. Therefore, establishing new therapeutic strategies to circumvent the chemoresistance and minimize treatment-associated toxicities is imperative.

Avenanthramide A (AVN A) belongs to the exclusive alkaloids of oats, and is one of the most abundant ingredients in avenanthramides (AVNs). AVN A displays better stability and bioavailability in plasma than other compounds after intake of AVNs-enriched food[7]. It exerts pleiotropic pharmacological activities such as antioxidation, anti-inflammation, antiatherosclerosis, immunomodulation, and anti-tumor. Our previous studies demonstrated that AVN A acts as a potential anticarcinogenic agent *via* causing an appreciable lethal induction of the already-elevated levels of ROS in CRC cells or activating the miR-129-3p/pirh2/p53 pathway to trigger CRC cell senescence specifically[8,9]. The pronounced features of AVN A such as lower toxicity, minimal side effects, and better bioavailability make it a promising candidate for adjuvant therapy to improve the overall therapeutic efficacy of certain first-line drugs synergistically. For this purpose, we focus on investigating the impact of AVN A on 5-FU-mediated therapeutic response in CRC.

miR-17-92 has been recognized as the first 'oncomir' encoded by *MIR17HG*, which contains six mature miRNAs: miR-17, miR-18a, miR-19a, miR-20a, miR-19b-1, and miR-92a-1[10,11]. Notably, the primary transcript of *MIR17HG* can undergo alternative splicing to produce three lncRNAs and among them, MIR17HG-202 and MIR17HG-203 generate miR-17-92. As an oncogenic cluster, miR-17-92 has been shown elevated in various cancer types including CRC. Indeed, several tumor suppressors are potent targets of miR-17-92, such as the proapoptotic factor Bim and tumor suppressor PTEN[11-14]. Notably, emerging evidence revealed the excessive expression of miR-17-92 in chemoresistant cells[15]. Accumulated evidence suggested that the epigenetic modifications are critical for regulating *MIR17HG* expression[16,17]. However, the regulatory relationship between Histone lysine demethylases (KDMs) and *MIR17HG* is still unclear.

KDMs execute a critical role in regulating transcriptional reprogramming by catalyzing the demethylation of histone lysine[18]. In general, histone H3 lysine 9 trimethylation (H3K9me3) is a mark typical of heterochromatin, which leads to transcriptional repression[19]. KDM4C is a histone demethylase that directly demethylates H3K9me3. Accumulating evidence have indicated elevated KDM4C level in various tumors which contribute to malignant transformation, genomic instability, DNA damage repair, tumor metastasis, and stemness maintenance[20,21].

Herein, we demonstrated a combinatorial anti-CRC activity of AVN A and 5-FU. AVN A treatment causes KDM4C degradation and thus reconfigures the occupation of H3K9me3 at *MIR17HG* promoter region. Subsequently, AVN A restrains the biogenesis of oncogenic miR-17-92 to liberate Bim expression. KDM4C/*MIR17HG*/GSK-3β negative feedback loop is critical for AVN A-mediated chemosensitization. Clinical specimens further confirm that the KDM4C/*MIR17HG*/GSK-3β negative feedback loop represents a crucial determinant of 5-FU response. Thus, our study proposes a promising alternative strategy to improve 5-FU efficacy towards chemoresistant CRC patients and provides novel therapeutic avenues that may be exploited to impinge on KDM4C/*MIR17HG*/GSK-3β negative feedback loop to circumvent chemoresistance.

2. Materials and methods

2.1. Chemicals and antibodies

AVN A was from Topharman (Shanghai, China). Cycloheximide (CHX) was from Solarbio (Beijing, China). The antibodies against Bim, Ubiquitin, GFP, and GSK-3β were purchased from Cell Signaling Technology (Beverly, MA, USA). Antibody for KDM4C was provided by Novus Biologicals (Littleton, CO, USA). Antibodies for H3K9me3 and GAPDH were obtained from Abcam (Cambridge, MA, USA). The antibodies against Bcl-2, Bcl-xL, Mcl-1, USP9X, Bik, PTEN, and LKB1 were purchased from Proteintech (Wuhan, China). The flag antibody was from Boster Biological Technology Co., Ltd. (Wuhan, China). PUMA antibody was bought from Bioss (Beijing, China).

2.2. Immunoblotting and ubiquitylation

The protein samples were subjected to SDS-PAGE and immunoblotting as described previously[8]. Following 24 h treatment with AVN A, cells were then incubated with 20 μmol/L MG-132 for 6 h to detect endogenous ubiquitination of KDM4C. Cell lysates were incubated with Protein A/G beads and KDM4C antibody overnight. KDM4C ubiquitination was determined by Western blot.

2.3. miRNA array

The miProfile TM human colorectal cancer miRNA array (GeneCopoeia, MD, USA) was applied for the characterization of

AVN A-mediated miRNA expression. The miRNA expression was normalized and analyzed by the $2^{-\Delta\Delta CT}$ method.

2.4. Chromatin immunoprecipitation (ChIP) assay

ChIP assays were conducted with a Kit from Millipore (Burlington, MA, USA) following the manufacturer's guidelines. After treatment, cross-linking of the cells was achieved with 1% formaldehyde, followed by sonication for generating DNA fragments with 150−900 bp. Antibodies for KDM4C, H3K9me3, and IgG were conducted for immunoprecipitation. Bound DNA fragments were subjected to PCR using the specific primers shown in Supporting Information Table S1.

2.5. Fluorescence in situ hybridization (FISH)

The FISH assay was conducted as previously reported[22]. Briefly, slices were dewaxed, rehydrated, pre-treated with hydrogen peroxide, and incubated with proteinase K. The digoxygenin (DIG)-labeled *MIR17HG* probe was synthesized by servicebio (Wuhan, China) and hybridization was carried out overnight at 37 °C. After washing, an anti-DIG-488 antibody (Servicebio, Wuhan, China) was used to react with the bound probe. DAPI was then used for counterstaining the nuclei. The signals were detected and analyzed with the DeltaVision Elite imaging system (GE, USA).

2.6. In vivo subcutaneous xenograft model and $Apc^{Min/+}$ mouse model

HCT-8 or HCT-8/FU (2×10^6 cells) were injected subcutaneously into the right flank of 4-week-old female nude mice. Upon reaching 100 mm^3, four groups of mice were randomly assigned: control, AVN A (15 mg/kg, 15 days, *p.o.*), 5-FU (20 mg/kg, 5 days, i.p.), or the AVN A/5-FU group. Calculating tumor volume was accomplished by: volume = length × $width^2/2$. Upon completion of the experiment, tumors were excised and weighted. Blood samples and tissues were collected for further examination. These animal experiments conformed to all relevant standards and were carried out upon approval of the Laboratory Animal Center & Nephrology, Shanxi Provincial People's Hospital (Shanxi, China).

The $Apc^{Min/+}$ mice (C57BL/6J-Apc^{Min}/J) were conducted with the approval of the Animal Ethics Committee of the Anhui Medical University. The $Apc^{Min/+}$ mice at 10 weeks of age were administered with 5-FU (20 mg/kg, i.p., for 5 consecutive days followed by 9 days of rest), AVN A (15 mg/kg, *p.o.*, every day), or in combination for 14 weeks. After treatment, mice were euthanized and polyps in the small intestine were counted under a stereomicroscope. The colon tumor number and tumor load were calculated. All animal care was in accordance with institutional guidelines.

2.7. Streptavidin−biotin affinity pull-down assay

HCT-8 cell lysates were incubated with streptavidin agarose beads (Yeasen Biotech, Shanghai, China) for 1 h at 4 °C. Then, free biotin or 10 μmol/L biotin-labeled AVN A (biotin-AVN A) was added and incubated with rotation overnight. Proteins bound to biotin-AVN A were pulled down with streptavidin agarose beads. After washing and boiling, the separation of denatured proteins was carried out using SDS-PAGE and staining by PAGE Gel Silver Staining Kit (Solarbio, Beijing, China). Differential protein bands were subjected to LC−MS/MS SHOTGUN assay by Shanghai Bioprofile Technology Company Ltd.

2.8. Cellular thermal shift assay (CETSA)

CETSA assay was performed as reported previously[23]. Cells were exposed to AVN A or an equal volume of vehicle. Then, cells were incubated in PBS which was supplied with Protease Inhibitor Cocktail (Seven Biotech, Beijing, China). The cells were aliquoted into tubes and heated at indicated temperatures for 3 min. Then, cells were frozen and thawed for three cycles in liquid nitrogen. After centrifugation, cell lysates were isolated by Western blot.

2.9. Microscale thermophoresis (MST) assay

His-KDM4C and His-KDM4C−S198M were purified and dyed with NT-647 *via* a kit of NanoTemper Technologies. The binding of AVN A to His-KDM4C, His-KDM4C−S198M was detected by Monolith NT.115 reader as reported[24].

2.10. Patient samples and establishment of patient-derived CRC organoids

Human CRC tissue specimens were sourced from the First Hospital of Shanxi Medical University (Taiyuan, China). All experiments using these specimens were approved by the ethics committee and informed consent was obtained from all patients. CRC tumor organoids were established according to previous reports[25]. Briefly, the freshly dissected tumor tissues were finely minced and dissociated into single-cell suspensions. The isolated CRC organoids were resuspended in Matrigel (BD Biosciences) and seeded in a 24-well plate and refreshed at 2−3 days intervals. After 6 days of incubation, 5-FU and AVN A were treated alone or together for 48 h on organoids. The relative number and size of tumor organoids were calculated.

2.11. Statistical analysis

The data were obtained from three independent experiments and analyzed by GraphPad Prism Software. Multiple comparisons were analyzed by One-way ANOVA followed by Tukey's post-test. The values were shown as the mean ± standard deviation (SD) or mean ± standard error of mean (SEM).

3. Results

3.1. AVN A synergizes with 5-FU in CRC cells

Given the fact that the dismal long-term clinical effects of individual therapy due to the inevitable cell resistance, we sought to investigate the therapeutic efficacy of combined treatment with AVN A and 5-FU in CRC cells. A substantial decline in cell viability was observed in the combined treatment group as compared to each AVN A or 5-FU treatment alone (Fig. 1A). The combination index (CI) was calculated by Calcusyn software[26] using a range of different concentrations of AVN A and 5-FU at a fixed ratio (about 4:3). The CI values at different effective concentration (EC) were all below 0.8 which strongly supporting that the combination of AVN A and 5-FU exhibited a synergistic effect (Fig. 1B and C). Furthermore, the synergy scores are calculated *via* SynergyFinder, combined treatment of AVN A and 5-FU exhibited a synergistic inhibitory effect (Supporting Information Fig. S1A). The combinatorial dose of AVN A (10 μmol/L) and 5-FU (7.5 μmol/L) with a death rate of over 50% was selected for follow-up experiments. In addition, compared to

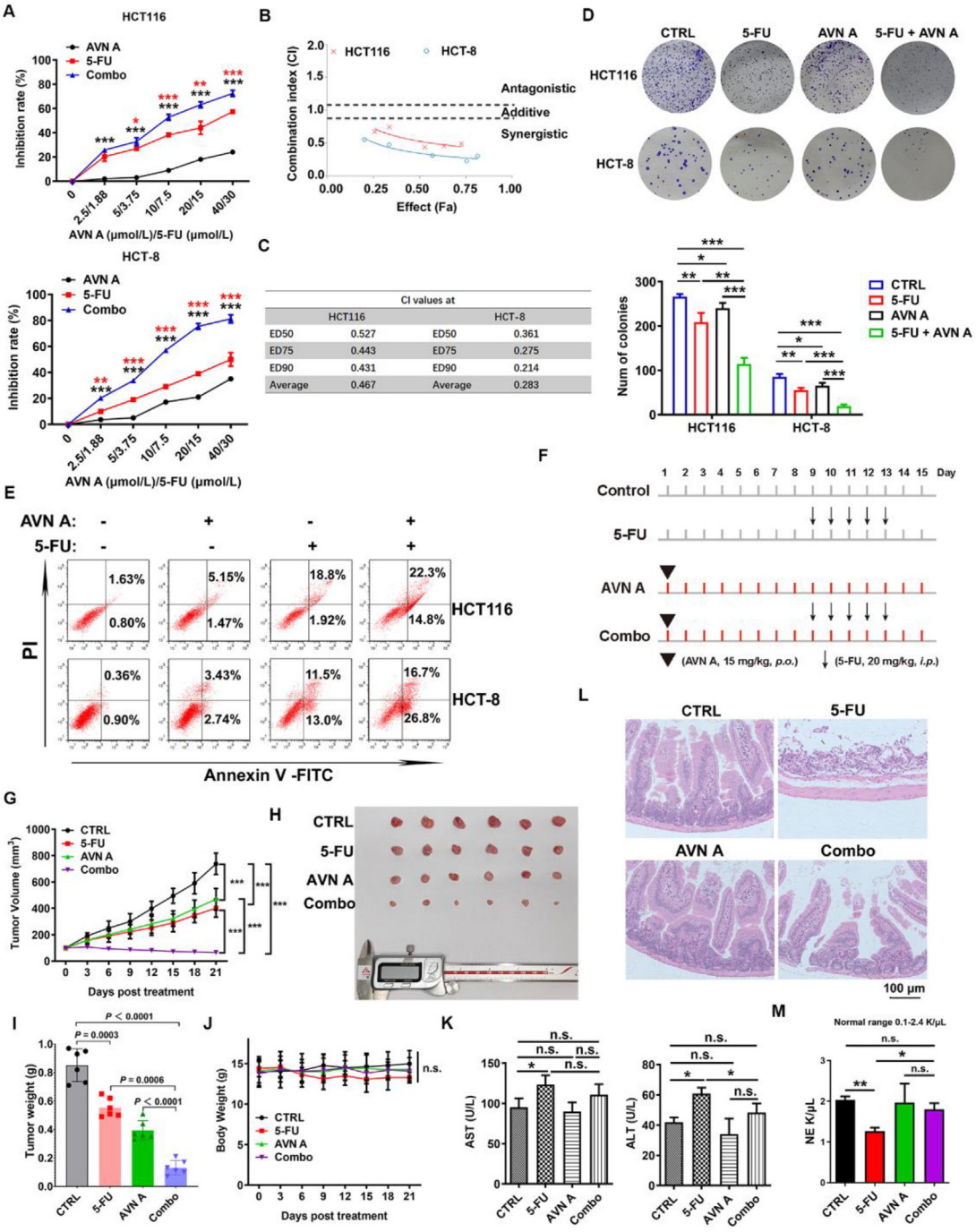

Figure 1 Combination of AVN A and 5-FU results in synergistic suppression of CRC cell growth. (A) Growth-inhibitory curves of CRC cells exposed to 5-FU and AVN A alone or together for 24 h. The black asterisk reveals the statistical significance between combo (refer to the combination of AVN A and 5-FU) and AVN A; the red asterisk reveals the statistical significance between combo and 5-FU, $n = 3$. (B) CI values for the entire fraction affected (Fa). (C) CI values at indicated points. (D) CRC cells were exposed to 5-FU (7.5 μmol/L) and AVN A (10 μmol/L) alone or together for 48 h, then analyzed by colony formation assay after 10 days (top panel). Relative colony numbers were presented as mean ± SEM (bottom panel), $n = 3$. (E) The combined effects of AVN A (10 μmol/L) and 5-FU (7.5 μmol/L) on the apoptotic CRC cells. (F) Schematic diagram showing the effect of AVN A, 5-FU, and the combination on tumor growth. (G−I) After subcutaneous inoculation with HCT-8 cells, nude mice were treated with 20 mg/kg of 5-FU, 15 mg/kg of AVN A, or both. The xenograft tumor growth curve (G) and tumor images (H) are shown. (I) Bar graph showing tumor weight. (J−M) Effects of combination strategies on body weight (J), AST and ALT (K), intestinal damage (L), NE counts (M). Data in (G)−(K), (M) are shown as mean ± SD, $n = 6$ per group; $^{*}P < 0.05$; $^{**}P < 0.01$; $^{***}P < 0.001$.

AVN A or 5-FU treatment alone, a combination of AVN A and 5-FU significantly suppressed CRC cell growth and induced cell apoptosis as demonstrated by colony formation (Fig. 1D) and annexin V/PI staining (Fig. 1E), respectively. The synergy of AVN A with other chemotherapeutic agents such as oxaliplatin or cisplatin (Fig. S1B and S1C) was also observed, albeit to a lesser extent than in combination with 5-FU.

To confirm the efficacy of AVN A on chemotherapy sensitization *in vivo*, BALB/c nude mice xenograft model was utilized (Fig. 1F). The data showed that the combined treatment provoked a remarkable retard on tumor growth than AVN A or 5-FU alone (Fig. 1G−I). Systemic adverse effects are still a major dilemma in the clinical application of 5-FU[3,27]. Subsequently, we asked whether AVN A could mitigate 5-FU-induced side effects. The combined dose was well tolerated and no weight loss was observed (Fig. 1J). Furthermore, the elevated liver enzyme activities of AST and ALT in the 5-FU treated group were partially reversed by AVN A treatment (Fig. 1K). H&E staining showed that 5-FU-induced intestinal injuries were improved by AVN A administration (Fig. 1L). In addition, 5-FU treatment significantly reduced neutrophil (NE) counts, whereas combination therapy could prevent neutropenia (Fig. 1M). Together, these data indicated that AVN A potentiates 5-FU therapeutic efficacy and alleviates systemic adverse effects of 5-FU in CRC.

3.2. *AVN A unleashes Bim by repressing the miR-17-92 cluster to enhance 5-FU efficacy in CRC cells*

Compelling evidence has indicated that dysregulation of apoptotic machinery determines the therapeutic responsiveness to 5-FU[28]. Our data showed that compared to other apoptosis-associated proteins, pro-apoptotic protein Bim was remarkably induced upon the combined treatment with AVN A and 5-FU (Fig. 2A and B). Research has shown that BIM-EL, BIM-L, and BIM-S are the three main subtypes that exert different pro-apoptotic potentials, and BIM-S is the most effective isoform in triggering cell apoptosis[29]. An obvious increase in all three forms of BIM was observed upon AVN A treatment (Fig. 2A and B). Actinomycin chase assay revealed that the degradation of *Bim* mRNA was blunted upon AVN A treatment compared to the control cells (Fig. 2C), suggesting that *Bim* mRNA underwent post-transcriptional regulation upon AVN A treatment.

MicroRNAs (miRNAs) are now recognized as key factors affecting mRNA stability[30]. A volcano plot from a small-scale miRNA array for 84 human CRC-related miRNAs showed three miRNAs (miR-17, miR-18a, and miR-20a) downregulated and two miRNAs (miR-183 and miR-451a) upregulated (Fig. 2D, Supporting Information Table S2). Importantly, these down-regulated miRNAs belong to the miR-17-92 cluster, which was dramatically reduced upon AVN A treatment (Fig. 2E). Mounting evidence highlights a link between the miR-17-92 cluster and tumor progression[11]. Thus, we next interrogated whether the miR-17-92 cluster is significantly differentially expressed in CRC. As expected, the upregulations of miR-17-92 cluster members were confirmed by analyzing the TCGA database (Fig. 2F and G).

Moreover, miR-17-92 cluster members share a substantial fraction of target genes including Bim[11]. MiR-92a was chosen randomly to verify whether Bim is a direct target of miR-17-92 as reported. We further confirmed that AVN A indeed attenuated miR-92a expression (Supporting Information Fig. S2A). TargetScan was performed to predict the putative binding sites for miR-92a. As shown in Fig. S2B, miR-92a mimics markedly reduced the luciferase activity of the wild-type Bim reporter rather than the mutant constructs. Moreover, AVN A enhanced 5-FU-induced upregulation of Bim expression, and CRC cell growth inhibition was partly abrogated by miR-92a overexpression (Fig. S2C and S2D). Notably, the expression of *MIR17HG* was decreased by AVN A treatment, indicating that AVN A impaired miR-17-92 expression at the transcriptional level (Supporting Information Fig. S3A). To elucidate the role of *MIR17HG* in CRC progression, TCGA data were analyzed by the online tool UALCAN. Strikingly, *MIR17HG* expression in CRC tissues was much higher than adjacent counterparts and displayed certain positive correlations with CRC clinical stages (Fig. 2H, Fig. S3B). Furthermore, the knockdown of *MIR17HG* resulted in a decrease of miR-17-92 cluster expression and an increase in Bim expression (Fig. 2I, Fig. S3C). AVN A increased the expression of PTEN and LKB1, which are validated targets of miR-17-92 (Fig. S3D). More importantly, treatment with 5-FU in *MIR17HG*-silenced CRC cells strongly potentiated chemotherapeutic response mimicking the synergistic effects of AVN A and 5-FU (Fig. 2J and K). Collectively, these findings indicated that AVN A restrains the transcription of *MIR17HG* to derepress Bim level which subsequently exacerbated 5-FU-induced apoptosis.

3.3. *AVN A directly binds to KDM4C to determine chemotherapeutic response in CRC*

To gain insights into how AVN A modulates the therapeutic response of CRC cells, we next identified directly targeted proteins of AVN A by purifying biotin-AVN A binding proteins from CRC cell lysates (Fig. 3A and B, Supporting Information Fig. S4A). Biotin-AVN A exhibited a similar activity as AVN A to enhance 5-FU sensitivity (Fig. S4B). The specific AVN A-bound proteins were analyzed and identified by SDS-PAGE and LC−MS/MS SHOTGUN assay, respectively (Fig. 3C and D). The results revealed that KDM4C and DDX3 were specifically retained by biotin-AVN A (Fig. 3C and D). Our previous work has shown that AVN A (50 μmol/L) directly binds to DDX3 to trigger ROS-mediated CRC cell apoptosis[7]. Considering the epigenetic role of histone demethylases KDM4C in target genes regulation[31], we showed *via* molecular dynamic (MD) simulations that AVN A could bind to KDM4C stably (Fig. 3E). CETSA results showed the thermal stability of KDM4C was enhanced with increasing temperatures upon AVN A treatment compared to the vehicle-treated group, which implied that AVN A bound to KDM4C (Fig. 3F). Moreover, the binding of AVN A to KDM4C was competed by free excess AVN A (Fig. 3G), and the ectopic expression of KDM4C rather than DDX3 abrogated AVN A-mediated chemosensitization (Fig. 3H, Fig. S4C). To decipher whether miR-129-3p is correlated to AVN A mediated 5-FU sensitization, HCT-8 cells were transfected with miR-129-3p mimics. We observed that overexpression of miR-129-3p did not significantly affect response to 5-FU in CRC cells (Fig. S4D). To further validate the direct binding of AVN A with KDM4C, the full-length of KDM4C was constructed and purified (Fig. 3I). As shown in Fig. 3J, surface plasmon resonance (SPR) analysis demonstrated a specific binding of AVN A to KDM4C with high binding affinity [affinity constant (K_D) = 7.985 μmol/L]. The results of TCGA database showed more pronounced KDM4C expression in CRCs compared to normal tissues (Fig. 3K). In agreement, the online LinkedOmics database further indicated that KDM4C level was negatively correlated with an overall survival rate of CRC patients (n = 376) (Fig. 3L). Importantly, AVN A exacerbated proapoptotic activity

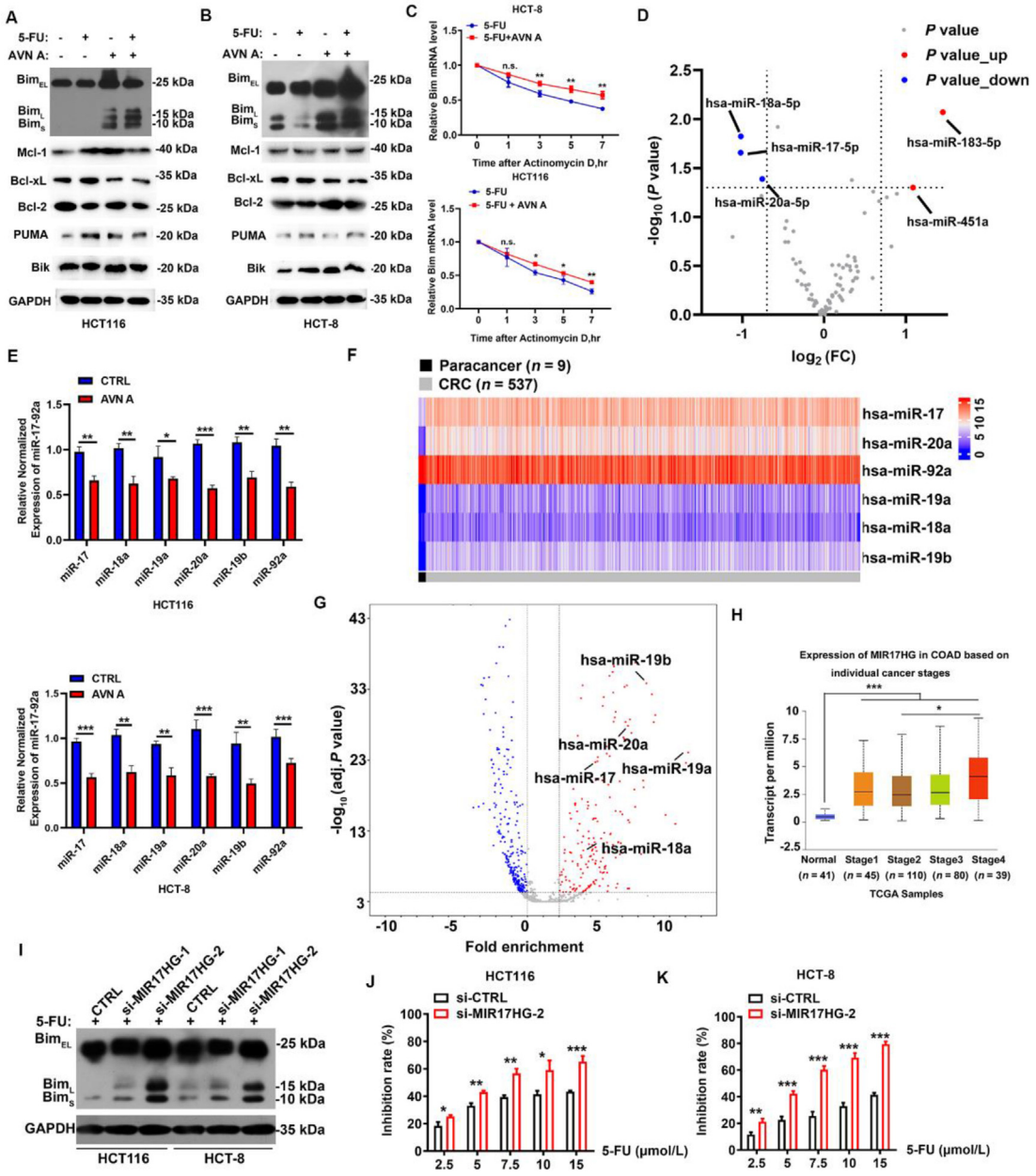

Figure 2 AVN A suppresses the miR-17-92 cluster to derepress Bim level. (A, B) HCT116 (A) and HCT-8 (B) cells were treated with 5-FU, AVN A, or combination for 24 h. Western blot was utilized for the levels of Bim, Mcl-1, Bcl-xL, Bcl-2, PUMA, and Bik. (C) CRC cells were exposed to 5-FU treatment alone and the combination and cultured with 1 μg/mL of actinomycin D for the indicated time. The mRNA stability of *Bim* was assessed using qPCR assay. (D) HCT-8 cells were treated with 5-FU and AVN A alone or together for 24 h and applied to qPCR analysis by miRNA array. Volcano plot demonstrates differentially expressed miRNAs *via* the combination of *P* values (cutoff = 0.05) and relative fold change (cutoff = 1.5). The downregulated miRNAs are shown in blue circles, whereas upregulated miRNAs are represented in red circles. (E) Following treatment with AVN A for 24 h, miR-17-92 cluster levels in CRC cells were analyzed by qPCR. (F) Heatmap of miR-17-92 cluster in the TCGA CRC database. (G) The differentially expressed miRNAs in 537 CRC samples and 9 adjacent normal tissues derived from TCGA are visualized in a volcano plot. The blue and red colors indicate low and high expression ($|\log2(\text{fold change})| > 1$, FDR <0.05), respectively. (H) The expression of *MIR17HG* in COAD based on individual cancer stage in TCGA CRC database. (I) Expression of Bim in CRC cells which transduced with two different si-*MIR17HG* (50 nmol/L) and then exposed to 5-FU for 24 h was detected by Western blot. (J, K) si-*MIR17HG* (50 nmol/L) was transferred into HCT116 (J) and HCT-8 (K) cells and then exposed to 5-FU for 24 h, and MTT assay was utilized to assess the relative cell viability. Data in (C)−(E), (J), (K) are shown as mean ± SD, $n = 3$; $^*P < 0.05$; $^{**}P < 0.01$; $^{***}P < 0.001$.

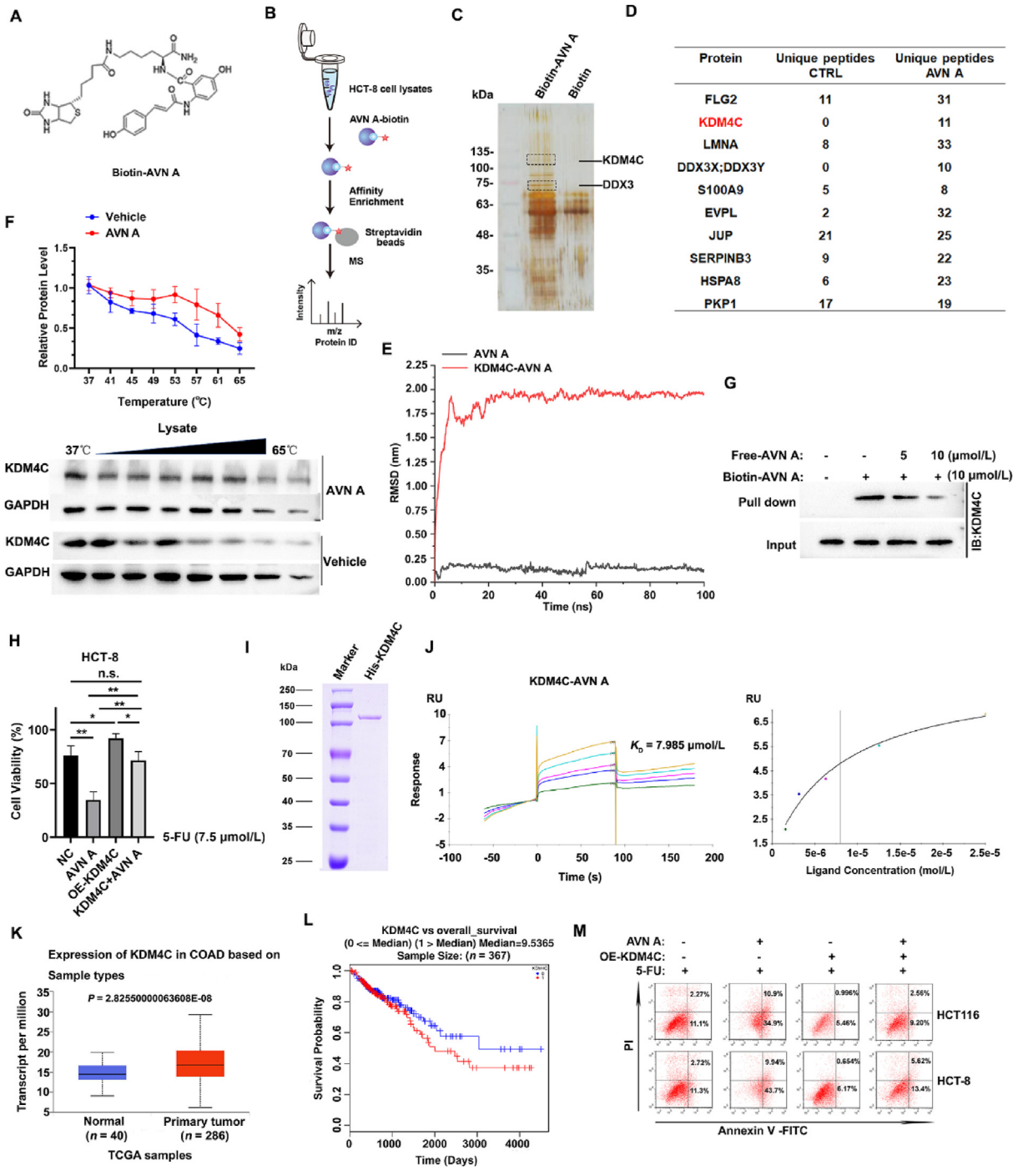

Figure 3 AVN A directly targets KDM4C and thereby critically mediates 5-FU response. (A) The chemical structure of biotin-AVN A was characterized. (B) A flowchart depicting the pulldown assay workflow with biotin-AVN A. (C) Representative silver-stained gel image of pulldown assay with biotin-AVN A in HCT-8 cells. (D) The top 10 proteins with the highest scores identified *via* LC−MS/MS SHOTGUN assay were listed. (E) Molecular dynamics simulation of AVN A binding to wild type of KDM4C. (F) Western bot analysis of CETSA of HCT-8 lysates that were incubated with AVN A (10 μmol/L) or an equal volume of the vehicle at the indicated temperature (bottom panel). The band intensity of KDM4C was derived from the Western blot results (upper panel). (G) Biotin or biotin-AVN A were added into HCT-8 cell lysates with free AVN A for 1 h, and then pulled down with streptavidin-agarose and analyzed by Western blot of the indicated protein. (H) The plasmids expressing KDM4C were transferred into HCT-8 cells and cell viabilities were assessed by MTT assay with 5-FU and AVN A alone or together for 24 h. (I) The full-length KDM4C was purified and determined by SDS-PAGE. (J) The binding affinities of KDM4C to AVN A were measured by SPR assay. (K) The expression of KDM4C in normal (n = 40) and primary tumor (n = 286) in the TCGA CRC database. (L) Kaplan−Meier survival analysis was performed to analyze CRC patients with low *vs* high levels of KDM4C (n = 367). (M) CRC cells were exposed to AVN A or OE-KDM4C in the presence of 5-FU (7.5 μmol/L). The apoptosis was determined by Annexin V/PI staining. Data in (F), (H) are shown as mean ± SD, n = 3; *$P < 0.05$; **$P < 0.01$.

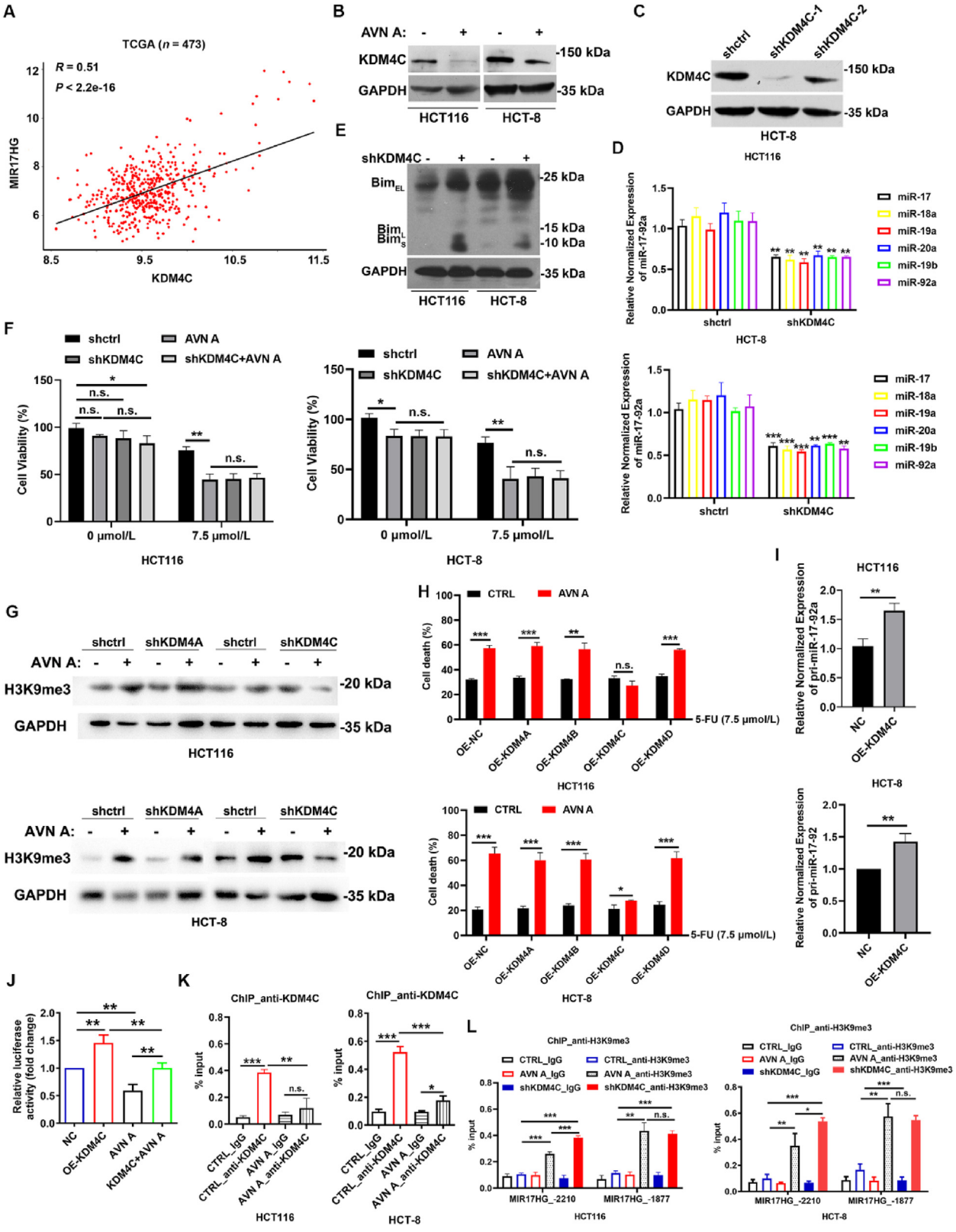

Figure 4 AVN A facilitates the enrichment of H3K9me3 at the *MIR17HG* promoter to derepress Bim expression *via* degrading KDM4C. (A) Scatter plots showing the correlations between KDM4C and *MIR17HG* in TCGA of CRC ($n = 473$). The Pearson correlation coefficients (r) and P values are shown. (B) KDM4C level in CRC cells treated with AVN A (10 μmol/L) was analyzed *via* Western blot. (C) KDM4C shRNAs or scramble shRNA was transferred into HCT-8 cells for 48 h. Then, the KDM4C level was detected by Western blot. (D) qPCR analysis of miR-17-92 cluster in HCT-8 cells after transfected with KDM4C shRNAs or scramble shRNA. (E) Bim level in CRC cells exposed to KDM4C shRNA or

of 5-FU was abrogated by KDM4C overexpression (Fig. 3M). Together, our results suggest that AVN A directly binds to KDM4C, which is an indispensable determinant for chemotherapeutic response in CRC.

3.4. AVN A fosters H3K9me3 occupancy on MIR17HG promoter to restrain its transcription via suppressing KDM4C

TCGA database analysis of the CRC cohort revealed a positive correlation between KDM4C and *MIR17HG* mRNA levels (Fig. 4A). As shown in Fig. 4B, KDM4C expression was suppressed upon AVN A treatment in CRC cells. To clarify whether miR-17-92 transcription was driven by KDM4C, we thus knocked down KDM4C expression in HCT-8 cells. The depletion of KDM4C remarkably attenuated the levels of miR-17-92 cluster members (Fig. 4C and D). Consistently, the protein level of Bim was elevated by KDM4C knockdown (Fig. 4E). Furthermore, the depletion of KDM4C phenocopied AVN A-mediated chemosensitization effects and AVN A-mediated chemosensitization was weakened by KDM4C silencing (Fig. 4F, Fig. S4E). Subsequently, we showed that knocking down KDM4C but not KDM4A abolished the AVN A-mediated upregulation of H3K9me3 in CRC cells (Fig. 4G).

To decipher the KDM4 subfamily member responsible for AVN A-mediated chemotherapy sensitization, we transfected CRC cells respectively with KDM4A, KDM4B, KDM4C, and KDM4D overexpression vectors (Fig. S4F). The cell death assay demonstrated that the overexpression of KDM4C rather than other KDM4 subfamily members abrogated AVN A-mediated chemosensitization (Fig. 4H). These data were further corroborated by the enhanced transcription level of *MIR17HG* in KDM4C overexpression CRC cells (Fig. 4I). To further explore whether KDM4C directly affected the transcription level of *MIR17HG*, luciferase reporters containing *MIR17HG* promoter region were constructed. As shown in Fig. 4J, AVN A impaired *MIR17HG* promoter luciferase activity was completely reinstated following the ectopic KDM4C expression. Additionally, the ChIP-qPCR assay revealed that the enrichment of KDM4C on the *MIR17HG* promoter was blunted by AVN A treatment (Fig. 4K). To determine whether the repressive mark H3K9me3 was enriched on *MIR17HG* promoter, ChIP-qPCR assay revealed a significant enrichment of H3K9me3 on *MIR17HG* promoter by either AVN A treatment or KDM4C silencing (Fig. 4L). Collectively, these findings demonstrate that AVN A remodels H3K9me3 occupancy on the *MIR17HG* promoter by suppressing KDM4C expression, which prevents biogenesis of oncogenic miR-17-92 cluster and leads to unleash Bim expression.

3.5. AVN A directly binds to S198 residue of KDM4C to abrogate MIR17HG transcription and dictate response to chemotherapy

To decipher the binding site of AVN A on KDM4C, the most favorable binding free energies, and top-ranked conformations were analyzed by molecular docking. The predicted result indicated that AVN A could form hydrogen bond with Ser198 and Asn200, and form salt bridge with Lys208 and His278 (Fig. 5A). Available studies have shown that S198 is essential for the demethylase activity of KDM4C, and the methionine substitution of Ser198 (S198M) is a catalytically inactive mutant of KDM4C[18]. To determine the responsible residue for AVN A-mediated chemosensitization effect, the above residues in the binding pocket of KDM4C were mutated (S198M, N200A, K208A, and H278A) and transfected into HCT-8 cells. Western blot analysis showed that AVN A mediated reduction in KDM4C expression in N200A, K208A, and H278A mutants rather than S198M mutant (Fig. 5B, Supporting Information Fig. S5A). Similar to the responses of HCT-8 cells in Fig. 4E, N200A, K208A, and H278A mutants, but not the S198M mutant, reacted to the combination of AVN A and 5-FU and shared a similar pattern of reduced cell viability and elevated cell death upon the combination treatment (Fig. 5C and D, Fig. S5B and S5C). Moreover, AVN A-mediated reduced levels of miR-17-92 cluster members were abrogated by S198M mutant overexpression rather than other mutants (Fig. 5E, Fig. S5D). Furthermore, pulldown assay on Streptavidin beads with wild type or KDM4C mutant constructs demonstrated that AVN A abundantly bound to KDM4C, N200A, K208A, and H278A mutants, but barely to the S198M mutant (Fig. 5F). Subsequently, the cellular MST assay reveals the interaction between AVN A and wild type or KDM4C−S198M mutant. As expected, the K_D value of the S198M mutant was much higher than that of wild type, indicating that the interaction of S198M mutant and AVN A was disappeared (Fig. 5G and H). In addition, AVN A resulted in the reduction of wildtype KDM4C protein rather than the mutant KDM4C−S198M protein. Increased KDM4C protein levels were observed followed by proteasome inhibitor MG-132 treatment in wildtype rather than mutant KDM4C−S198M cells (Fig. 5I). The CHX assay demonstrated that AVN A treatment facilitated the degradation rate of the endogenous KDM4C (Fig. 5J). Indeed, our findings indicated that AVN A treatment resulted in increased ubiquitination in wildtype KDM4C protein rather than the mutant KDM4C−S198M protein, suggesting that AVN A-mediated KDM4C degradation relies on the ubiquitin/proteasome pathway and KDM4C−S198M resist these effects of AVN A (Fig. 5K).

scramble shRNA for 48 h was detected *via* Western blot. (F) KDM4C shRNA or scramble shRNA was transferred into CRC cells and exposed to 5-FU and AVN A alone or together for 24 h. Cell viabilities were assessed by MTT assay. (G) CRC cells were transfected with KDM4A shRNA or KDM4C shRNA after incubating with AVN A for 24 h H3K9me3 level was then detected *via* Western blot. (H) The plasmids expressing KDM4A, KDM4B, KDM4C, and KDM4D were transferred into CRC cells and exposed to AVN A and 5-FU together for 24 h. Trypan blue staining was conducted to measure cell death. (I) The plasmids expressing GFP-tagged KDM4C were transferred into CRC cells and the *MIR17HG* level was detected *via* qPCR analysis. (J) The *MIR17HG* reporter constructs were treated with GFP-KDM4C, AVN A, or in combination for 48 h in HEK293T. We then evaluated and normalized the luciferase activities against Renilla luciferases. (K) CRC cells were exposed to AVN A (10 μmol/L) and then ChIP-qPCR was conducted to assess KDM4C levels on the *MIR17HG* promoter. (L) ChIP-qPCR was conducted to assess H3K9me3 levels at the *MIR17HG* promoter in CRC cells exposed to AVN A (10 μmol/L) or transfected with KDM4C shRNAs. Data in (D), (F), (H)−(L) are shown as mean ± SD, $n = 3$; *$P < 0.05$; **$P < 0.01$; ***$P < 0.001$.

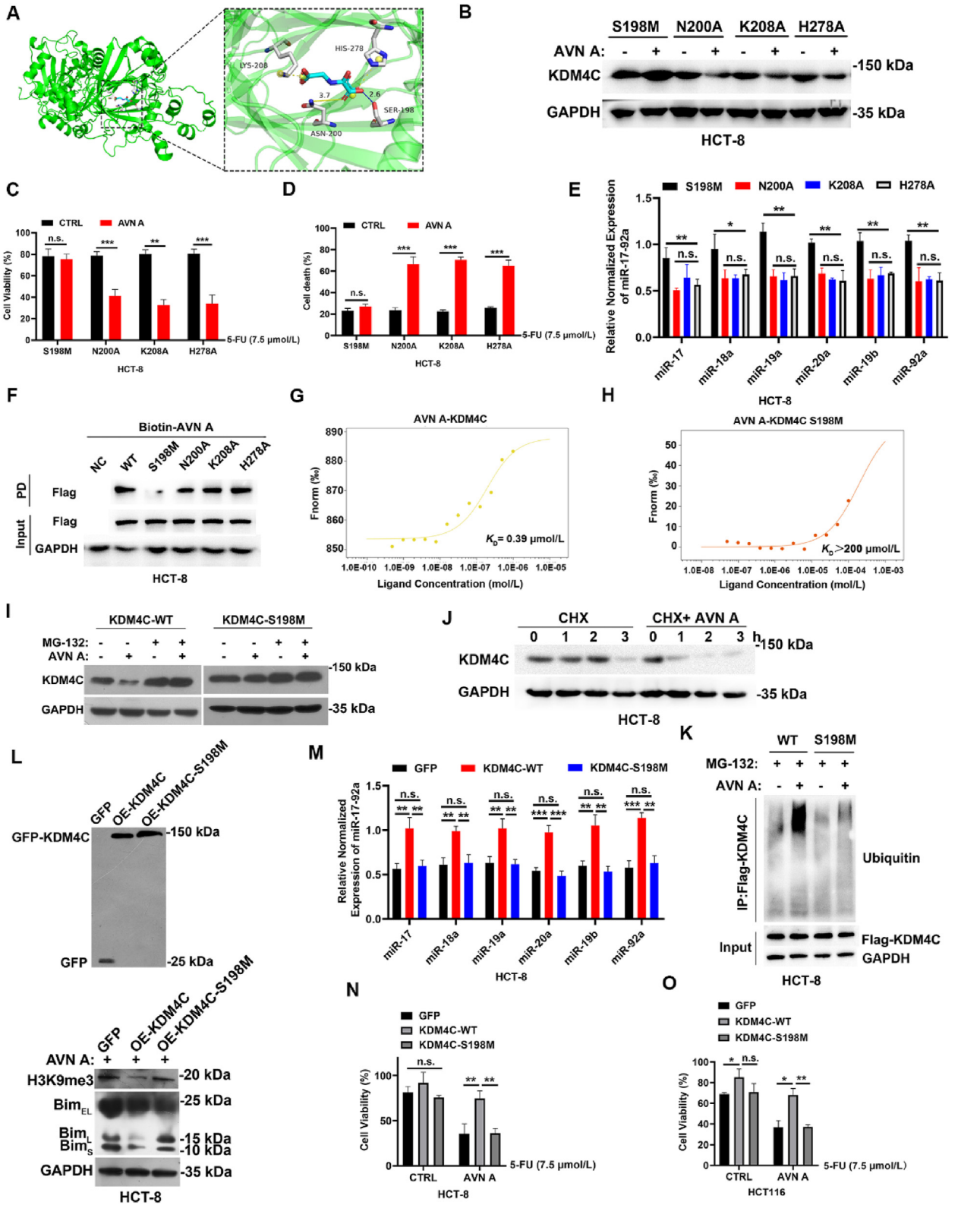

Figure 5 AVN A directly targets KDM4C at S198 to restrain *MIR17HG* transcription to improve 5-FU sensitivity. (A) Molecular docking was utilized to decipher the interaction of AVN A and KDM4C. (B) The four KDM4C site mutants were transferred into HCT-8 cells and then exposed to AVN A and 5-FU alone or together for 24 h KDM4C level was evaluated *via* Western blot. (C, D) Cells were exposed to AVN A and 5-FU for 24 h and cell viability (C) and cell death (D) were analyzed *via* MTT assay and trypan blue staining. (E) The four KDM4C site mutants were transferred into HCT-8 cells with AVN A treatment for 24 h miR-17-92 cluster levels were determined *via* qPCR. (F) The flag-tagged wild type or

Notably, AVN A-mediated expression of Bim and H3K9me3 can be reverted by KDM4C overexpression rather than KDM4C−S198M (Fig. 5L). In addition, the suppressive effect of AVN A on miR-17-92 cluster biogenesis depends on the demethylase activity of KDM4C, since KDM4C−S198M was unable to abrogate AVN A-mediated transcriptional repression of miR-17-92 cluster (Fig. 5M). We further explored the role of KDM4C demethylase activity in AVN A-mediated chemotherapy response. The synergistic effect of combination therapy on CRC cells was compromised by KDM4C overexpression but not KDM4C−S198M (Fig. 5N and O). These data collectively suggest that AVN A exerts its chemosensitizing effect by directly targeting S198 of KDM4C to block *MIR17HG* transcription and derepress Bim expression.

3.6. AVN A improved the therapeutic efficacy of 5-FU via impairing KDM4C/MIR17HG/GSK-3β negative feedback loop

Our mechanistic studies revealed that AVN A-mediated KDM4C degradation mainly *via* ubiquitin/proteasome pathway (Fig. 5I−K). Available studies have shown that the deubiquitinase USP9X facilitates KDM4C expression by mediating the deubiquitination of KDM4C to accentuate the malignant progression of lung cancer[32]. Recent studies have also revealed that the activation of glycogen synthase kinase 3β (GSK-3β) promotes the interaction of the ubiquitin ligase β-TrCP and KDM4C to induce KDM4C degradation[21]. Accordingly, our results demonstrated that AVN A treatment obviously promoted GSK-3β level and hardly influenced the expression of USP9X (Fig. 6A and B). Moreover, the knockdown of GSK-3β in CRC cells significantly revoked the reduced KDM4C and increased GSK-3β caused by AVN A treatment (Fig. 6C and D). Numerous studies have demonstrated that miR-19a and miR-20a can directly target and inhibit GSK-3β expression[33,34]. It prompted us to speculate that *MIR17HG* can directly suppress the levels of GSK-3β. The results showed that AVN A-mediated upregulation of GSK-3β was reversed in *MIR17HG* overexpressing CRC cells (Fig. 6E, Fig. S4G), and overexpression of KDM4C rather than S198M mutant abrogated AVN A-mediated the upregulation of GSK-3β level (Fig. 6F). The co-immunoprecipitation results further revealed that AVN A treatment significantly promoted the interaction between KDM4C, but not the S198M mutant, and β-TrCP, and subsequently promoted the ubiquitination of KDM4C (Fig. 6G). In addition, the knockdown of GSK-3β reduced AVN A-mediated chemosensitization, which was fully rescued by silencing of KDM4C or *MIR17HG* (Fig. 6H and I). Collectively, these findings demonstrate that AVN A directly targets S198 of KDM4C to exert chemosensitization effects *via* suppressing the KDM4C/*MIR17HG*/GSK-3β negative feedback loop (Fig. 6J).

3.7. AVN A reversed 5-FU resistance in HCT-8/FU cells-derived xenografts

The AOM/DSS mouse model used in our previous study was applied to evaluate the effect of AVN A on KDM4C/*MIR17HG* expression[8]. As shown in Supporting Information Fig. S6A, KDM4C level was significantly reduced whereas Bim expression was notably increased upon AVN A treatment. Moreover, the FISH assay revealed that mice administrated with AVN A typically accompanied by the attenuation of *MIR17HG* compared to the AOM/DSS group (Fig. S6B). To verify whether AVN A could overcome 5-FU resistance *in vivo*, the HCT-8/FU-derived xenografts model was utilized for further investigations. Although 5-FU or AVN A alone only slightly suppressed tumor growth, the combined treatment resulted in complete inhibition of tumor growth (Fig. 7A−C). The results revealed that KDM4C and *MIR17HG* levels were significantly reduced, Bim and GSK-3β levels were notably increased compared to 5-FU or AVN A treatment alone (Fig. 7D). Moreover, in the combinatorial treatment group, good tolerance, and no appreciable weight loss was observed (Fig. 7E). In addition, no major pathological changes in the cellular morphology of the normal tissues and organs (liver, spleen, lungs, kidneys) were detected (Fig. 7F). The data was further supported by H&E staining demonstrated that 5-FU mediated liver injury can be alleviated by combined treatment (Fig. 7F). These findings thus suggested that improved efficacy of AVN A and 5-FU combined treatment in chemoresistant xenograft tumors *in vivo*.

3.8. AVN A bolsters the chemotherapy response in $Apc^{Min/+}$ mice and CRC organoid model

To further confirm AVN A-sensitized CRC to 5-FU, an $Apc^{Min/+}$ mouse model, which predominantly spontaneously develops intestinal adenomas, was utilized. $Apc^{Min/+}$ mice were administered with 5-FU, AVN A, or in combination for 14 weeks and evaluated by tumor number and tumor load (Fig. 8A and B). Representative H&E staining and macroscopic results revealed that the 5-FU and AVN A combined treatment developed fewer and smaller intestinal polyps, a noticeable reduction of tumor number and tumor burden compared to the 5-FU group or AVN A group (Fig. 8C−E). Furthermore, the CRC patient-derived organoid (PDO) model exhibited more robust responses to the combined treatment compared to the treatment with either 5-FU or AVN A alone (Fig. 8F−I). Altogether, our data provide evidence for improving 5-FU efficacy in CRC with the combination of AVN A in CRC organoid and $Apc^{Min/+}$ mice model.

indicated mutant of KDM4C constructs was transferred into HCT-8 cells. Cell lysates were then analyzed by the Streptavidin-pull down assay. (G, H) The high-affinity interactions of AVN A and wild-type (WT) KDM4C (G) or S198M (H) were evaluated *via* MST assay. (I) HCT-8 cells with transfection of wild type or mutant of KDM4C constructs that were exposed to AVN A (10 μmol/L), MG-132 (20 μmol/L), or combination for 24 h KDM4C was detected *via* Western blot. (J) Western blot analysis of KDM4C in HCT-8 cells exposed to AVN A with 20 μmol/L CHX at various times. (K) The WT KDM4C or S198M vectors were transferred into HCT-8 cells and treated with AVN A in the presence of MG-132 for ubiquitination analysis. (L) HCT-8 cells were transfected with plasmids expressing GFP, KDM4C, or S198M with AVN A treatment for 24 h, and levels of H3K9me3 and Bim were determined. (M) The plasmids expressing GFP, KDM4C, or S198M were transferred into HCT-8 cells with AVN A treatment for 24 h. The miR-17-92 cluster levels were determined *via* qPCR. (N, O) The GFP-KDM4C or S198M plasmids were transferred into HCT-8 (N) and HCT116 cells (O) and exposed to 5-FU and AVN A alone or together for 48 h. Cell viabilities were determined *via* MTT assay. Data in (C)−(E), (M)−(O) are shown as mean ± SD, $n = 3$; $^{*}P < 0.05$; $^{**}P < 0.01$; $^{***}P < 0.001$.

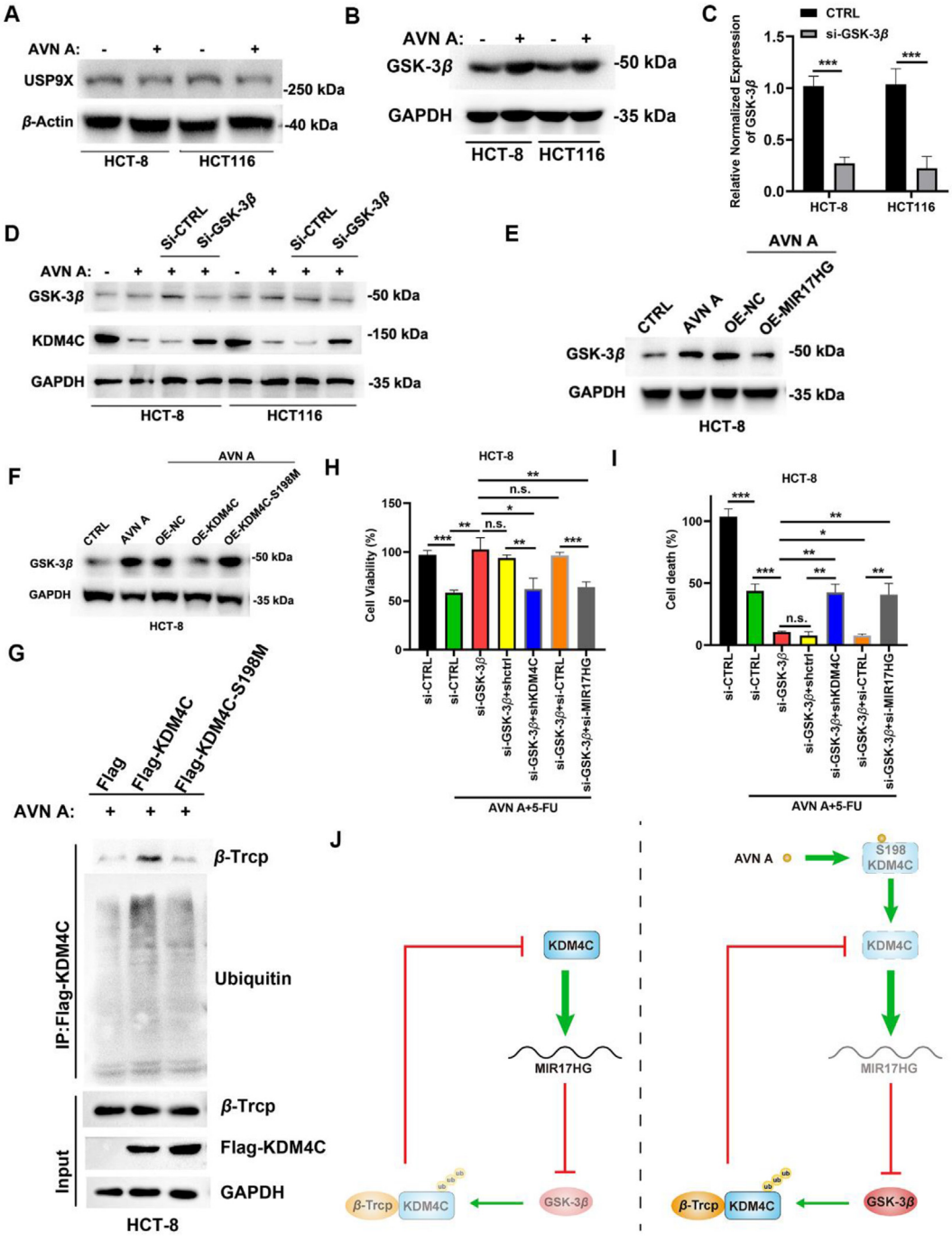

Figure 6 AVN A enhances 5-FU efficacy *via* targeting the KDM4C/*MIR17HG*/GSK-3β negative feedback loop. (A, B) Levels of USP9X (A) and GSK-3β (B) in CRC cells upon AVN A (10 μmol/L) treatment were determined *via* Western blot. (C) The siRNA against GSK-3β was transferred into HCT-8 cells for 48 h and GSK-3β levels were determined by qPCR. (D) CRC cells which transfected with si-CTRL or si-GSK-3β with 10 μmol/L AVN A for 24 h and analyzed *via* Western blot. (E) The plasmids of OE-NC or OE-*MIR17HG* were transferred into HCT-8 cells with 10 μmol/L AVN A for 24 h. GSK-3β levels were determined by Western blot. (F) The WT KDM4C or S198M constructs were transferred into HCT-8 cells and exposed to 10 μmol/L AVN A for 24 h. GSK-3β levels were determined by Western blot. (G) The WT KDM4C or S198M vectors were transferred into HCT-8 cells and exposed to 10 μmol/L AVN A for 24 h with MG-132 (20 μmol/L). Immunoprecipitation was conducted using a flag antibody. (H, I) HCT-8 cells expressing si-GSK-3β with shKDM4C or si-MIR17HG were exposed to 10 μmol/L AVN A and 7.5 μmol/L 5-FU for 24 h. MTT assay and the trypan blue staining were performed to detect cell viabilities (H) and cell death (I). (J) A model illustrating the KDM4C/*MIR17HG*/GSK-3β negative feedback loop mediated by AVN A. Data in (C), (H), (I) are shown as mean ± SD, $n = 3$; $^{*}P < 0.05$; $^{**}P < 0.01$; $^{***}P < 0.001$.

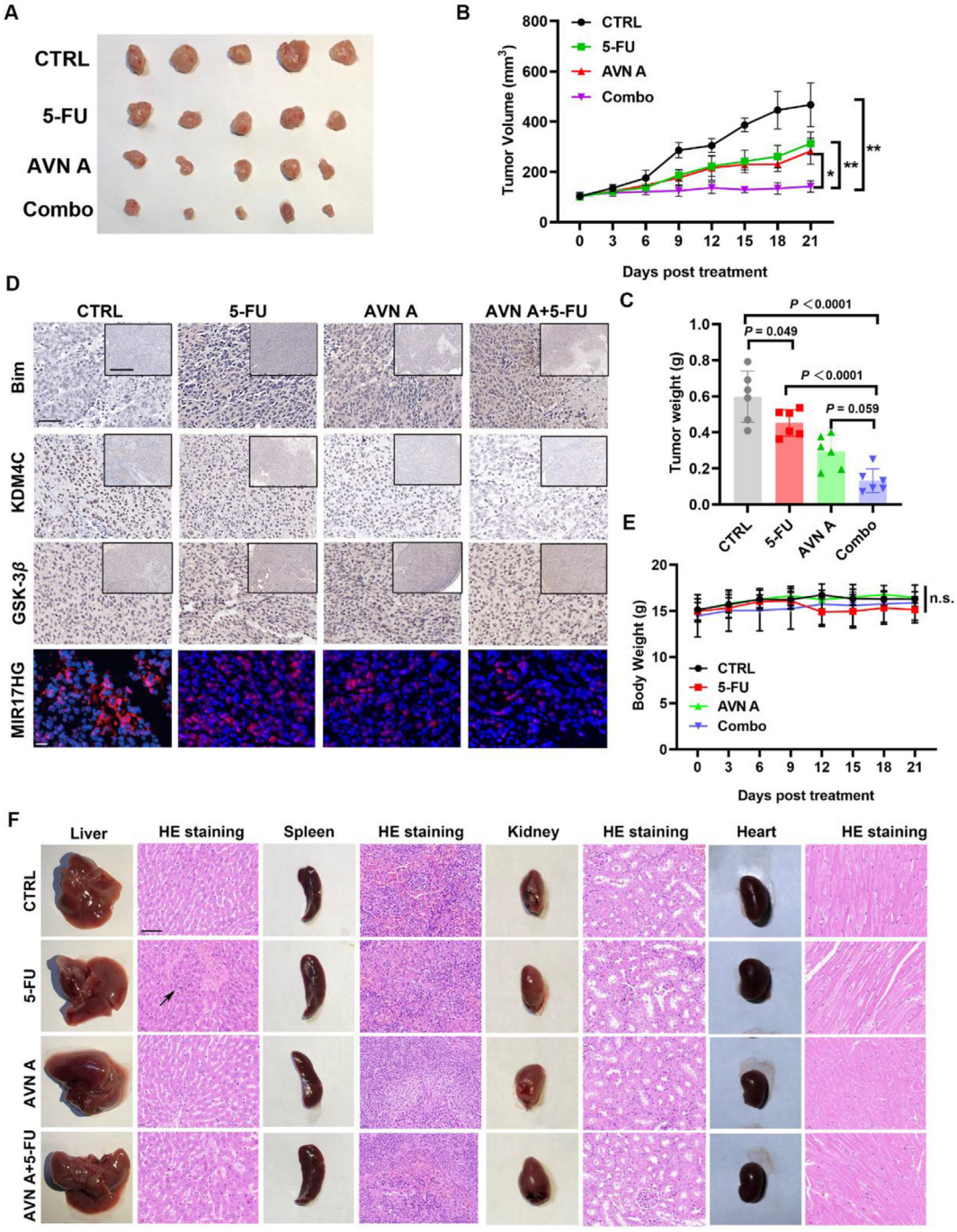

Figure 7 AVN A reversed 5-FU resistance in HCT-8/FU cells-derived xenografts. (A–C) Nude mice subcutaneously inoculated with HCT-8/FU cells were administered with the vehicle, 5-FU (20 mg/kg), AVN A (15 mg/kg), or both. The representative photos of HCT-8/FU xenografts (A), xenograft tumor volume (B), and tumor weight (C) are shown. (D) IHC staining results for KDM4C, GSK-3β, and Bim staining in tumor samples from the indicated groups (top panel). Representative FISH images of *MIR17HG* in tumor samples (bottom panel). Scale bars, 50 μm (main) and 500 μm (inset). Scale bars for FISH, 10 μm. (E) The body weight was evaluated during the treatment. (F) H&E staining analysis of the liver, spleen, kidney, and heart of HCT-8/FU cells-derived xenografts. Scale bars represent 50 μm. Data in (B), (C), (E) are shown as mean ± SD, $n = 6$; $^{*}P < 0.05$; $^{**}P < 0.01$.

3.9. The KDM4C/MIR17HG/GSK-3β negative feedback loop serves as predictive biomarkers of 5-FU response

To further clarify the clinical relevance of KDM4C/*MIR17HG* and 5-FU resistance, a cohort of 31 CRC patients who received 5-FU-based therapy were evaluated by IHC and FISH (Fig. 9A). All the patients were grouped according to the response to 5-FU, where patients 1–17 with recurrence were considered as "resistant" and patients 18–31 who remained free of disease since the initial treatment were considered as "sensitive" (Table 1). Based on the homology region of human and mouse *MIR17HG*, a specific oligonucleotide probe with shared transcribed region on

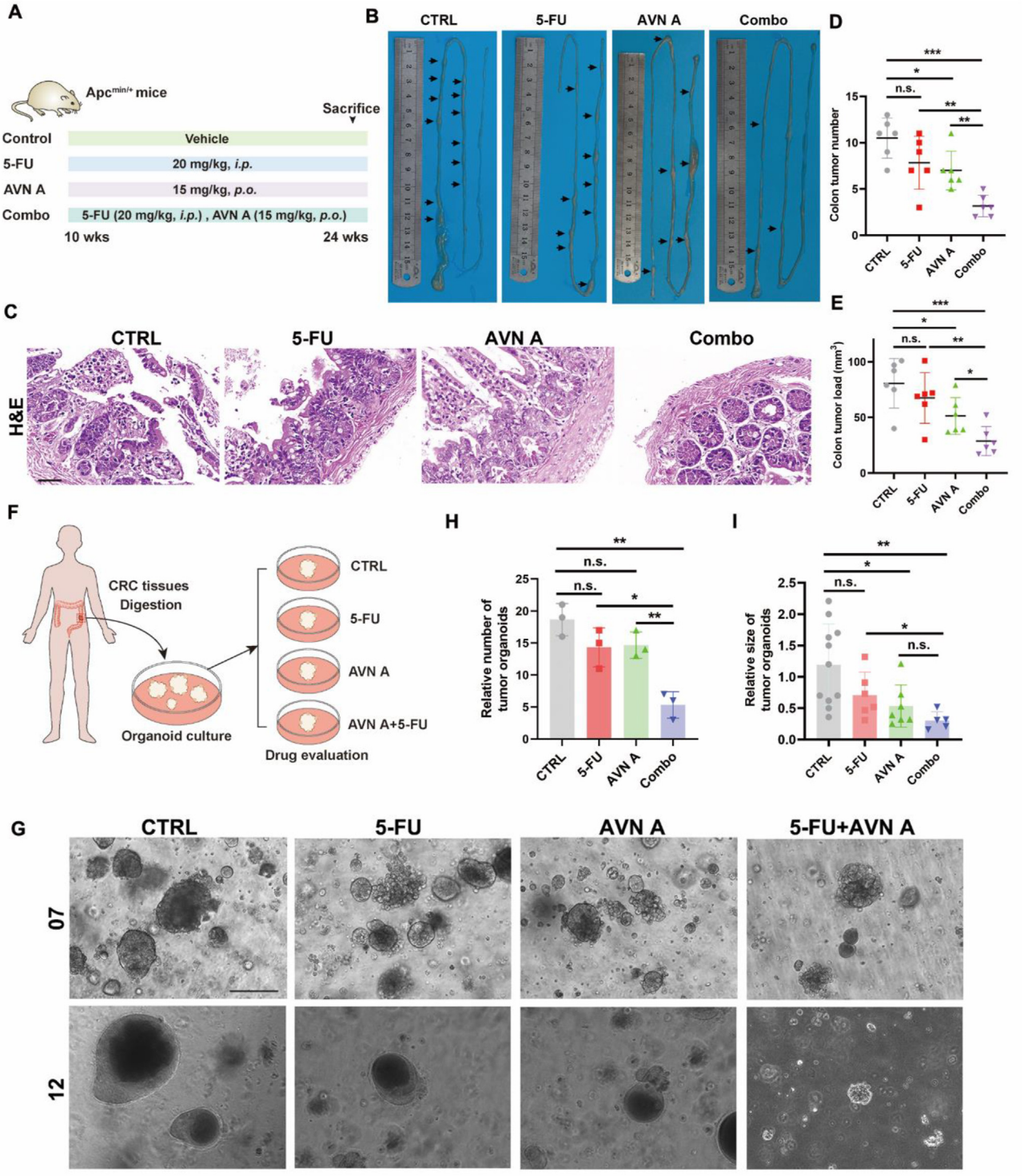

Figure 8 The efficacy of 5-FU is enhanced by AVN A in $Apc^{Min/+}$ mice and the CRC organoid model. (A) Schematic diagram of 5-FU, AVN A, or combination on tumorigenesis of $Apc^{Min/+}$ mice. (B) Macroscopic images of small intestines from $Apc^{Min/+}$ mice exposed to 5-FU, AVN A, or combination for 14 weeks. (C) H&E staining of $Apc^{Min/+}$ mice colons. Scale bars, 50 μm. (D, E) Tumor number (D) and tumor load (E) from $Apc^{Min/+}$ mice exposed to 5-FU, AVN A, or combination were analyzed. (F) Workflow of CRC organoids-based drug evaluation. (G) CRC organoids after 6 days of culture were treated with 5-FU (7.5 μmol/L) and AVN A (10 μmol/L) alone or their combination for 48 h. Representative images were recorded by microscope. Scale bars, 500 μm. (H, I) The relative number of tumor organoids (H) and relative size of tumor organoids (I) were calculated from (G). Data in (D), (E) are shown as mean ± SD, $n = 6$. Data in (H) are shown as mean ± SD, $n = 3$; $^{*}P < 0.05$; $^{**}P < 0.01$; $^{***}P < 0.001$.

MIR17HG-202 and *MIR17HG*-203 was designed to detect *MIR17HG* expression. The levels of KDM4C and *MIR17HG* were significantly higher in patients who progressed on 5-FU compared with the sensitive group (Fig. 9B and D). Conversely, the decreased Bim and GSK-3β expression was observed in tumors that advanced on 5-FU-based therapy (Fig. 9B, C and E) Of note, *MIR17HG* expression showed respectively a positive correlation with KDM4C expression, and inverse correlations with Bim expression and GSK-3β expression, respectively (Fig. 9F−H). CRCs with microsatellite instability (MSI) status have been reported to respond poorly to FU-based chemotherapy[35]. The Genomics of Drug Sensitivity in Cancer Project datasets (GDSC) was conducted to evaluate the effect of KDM4C on the chemotherapeutic response of CRC cells. As shown in Fig. 9I, KDM4C levels exhibited a significant positive correlation with the IC_{50} to 5-FU in MSI CRC cells, indicating that KDM4C^{high} CRC patients did not benefit from 5-FU-based adjuvant chemotherapy. The results of Kaplan−Meier Plotter showed that a high level of GSK-3β was correlated with a shorter overall survival (Fig. S6C). Additionally, Kaplan−Meier curves demonstrated that the subgroup with KDM4C^{high}/*MIR17HG*^{high} was correlated with a poor prognosis for CRC patients in the TCGA cohort (Fig. 9J). Collectively, these data potentially link the KDM4C/*MIR17HG*/GSK-3β negative feedback loop to 5-FU response in CRC patients.

4. Discussion

Epidemiological reports indicated that daily consumption of oats can reduce the risk of cancer[36]. As a unique phytochemical in oats, AVNs have attracted substantial attention from academic research and pharmaceutical companies due to their numerous health benefits. Structural analogs of AVNs such as tranilast have been approved for allergic disease treatment[37]. The compensatory features such as low toxicity, good safety, and high bioavailability make AVN A as a promising adjuvant component to improve the efficacy of first-line chemotherapy drugs. Here, we evaluated the effect of AVN A on chemotherapy response and revealed the underlying molecular mechanisms.

Resistance to anticancer drugs is a major obstacle to achieving effective cancer therapy. Dysregulation of apoptosis-related proteins expression is regarded as an important tumor resistance mechanism[38]. Available studies have shown that combining phytochemicals with first-line chemotherapeutics will eliminate cancer cells *via* elevating apoptosis and subsequently blunt the emergence of drug resistance, representing a more effective anticancer strategy[39]. Notably, the pro-apoptotic protein Bim was significantly upregulated after AVN A treatment, which strongly potentiates the 5-FU therapeutic efficacy (Fig. 2A and B). We found that the combination of AVN A and 5-FU is a potential strategy to maximize the induction of Bim, which is a proapoptotic sentinel that mediates Bax/Bak-dependent apoptosis. More importantly, the combination of AVN A with oxaliplatin or cisplatin is still effective in CRC cells (Fig. S1B and S1C), indicating the broad applicability of this combined strategy to a variety of first-line regimens for CRC.

The miR-17-92 cluster is highly expressed in various tumors and exerts oncogenic potential[40,41]. Most targets of miR-17-92 cluster members are “tumor killers”. For example, Bim is targeted by all individual members of the cluster; PTEN is the target of miR-19; and LKB1 tumor suppressor is negatively regulated by miR-17 and miR-20[42]. Together, the miR-17-92 network exacerbated tumor progress in multiple aspects primarily attributed to their targets. Additionally, the miR-17-92 cluster members share most target genes. Obviously, blocking one cluster member might initiate compensatory mechanisms by other miRNAs. A previous report developed a novel locked nucleic acid (LNA) gapmeRs called MIR17PTi to globally inhibit the miR-17-92 cluster and found that the miR-17-92-based therapeutic strategy has clinical translational value in multiple myeloma[11]. Unlike LNAs that are limited by delivery efficiency challenges, we found that AVN A impaired miR-17-92 cluster at 24 h *via* impeding *MIR17HG* transcription rather than inhibiting its individual member, which destroyed the compensatory pathway (Fig. 2E). Consequently, AVN A enabled depression of the shared target protein Bim of *MIR17HG*, thus achieving the lethal effect in combination with 5-FU (Fig. 2I−K). This study proposes that targeting *MIR17HG* as the Achilles heel of CRC, which could be a key feasible strategy to improve the response to chemotherapy in CRC.

Natural products are an important source of new drug development, and the identification of their targets is crucial for elucidating the mechanism of drug action. Here, we demonstrated that AVN A directly bound to KDM4C by biotin affinity pulldown, CETSA, and SPR (Fig. 3B, C, F, and J). As a H3K9 demethylase, KDM4C is highly expressed in various tumors and regulates gene transcription by remodeling chromatin and altering histone methylation levels[26]. To our knowledge, no study has reported the regulatory role of KDM4C on *MIR17HG*. Our data showed that KDM4C plays a critical role in AVN A-mediated transcriptional repression of *MIR17HG* (Fig. 4D), and thus ascertained a novel proto-oncogenic role of KDM4C. KDM4C could be recruited to the *MIR17HG* promoter region to facilitate *MIR17HG* transcription in a histone demethylase-dependent manner, thereby attenuating its downstream tumor suppressor gene expression (Fig. 4G−J). This raised an interesting question of interaction mechanisms by which AVN A specifically acts on KDM4C. We uncovered that AVN A directly binds to the S198 site of the methylase activity of KDM4C, which sequentially attenuated its demethylase activity and induced KDM4C degradation (Fig. 5A−E). AVN A-mediated repression of KDM4C upregulates the occupancy of H3K9me3 in the promoter region of *MIR17HG*, thereby repressing *MIR17HG* transcription and derepressing its target protein Bim. Our findings illustrate the potential druggability of KDM4C and provide a molecular basis for targeting KDM4C with natural compounds. Accumulating evidence have demonstrated that some small molecules can directly bind to a specific protein to induce its degradation[43,44]. It has been reported that USP9X-mediated KDM4C deubiquitination facilitates lung cancer progression[32]. In addition, GSK-3β facilitates the interaction of the ubiquitin ligase β-TrCP and KDM4C to trigger KDM4C ubiquitination and degradation[19]. High expression and activation of tumor suppressor GSK-3β has been reported to diminish anti-apoptotic protein MCL-1 levels to induce tumor cell death and attenuate tumor growth[45]. Our findings uncovered that AVN A enhances Bim-mediated chemosensitization of CRC *via* targeting KDM4C/*MIR17HG*/GSK-3β negative feedback loop (Fig. 10).

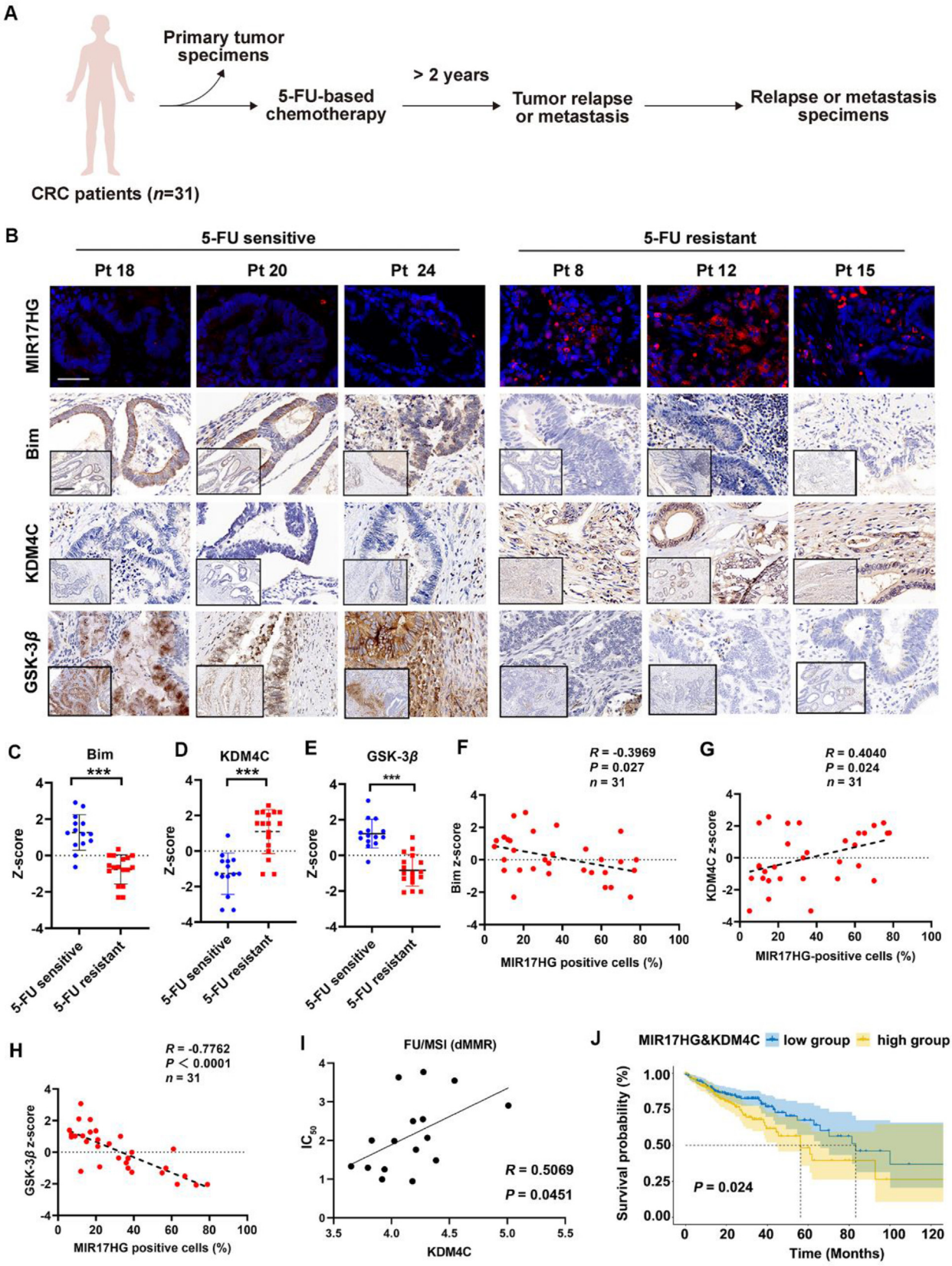
A
Primary tumor specimens
5-FU-based chemotherapy
> 2 years
Tumor relapse or metastasis
Relapse or metastasis specimens
CRC patients (n=31)
B
5-FU sensitive
5-FU resistant
Pt 18
Pt 20
Pt 24
Pt 8
Pt 12
Pt 15
MIR17HG
Bim
KDM4C
GSK-3β
C
Bim
***
Z-score
5-FU sensitive
5-FU resistant
D
KDM4C
***
Z-score
5-FU sensitive
5-FU resistant
E
GSK-3β
***
Z-score
5-FU sensitive
5-FU resistant
F
R = -0.3969
P = 0.027
n = 31
Bim z-score
MIR17HG positive cells (%)
G
R = 0.4040
P = 0.024
n = 31
KDM4C z-score
MIR17HG-positive cells (%)
H
R = -0.7762
P < 0.0001
n = 31
GSK-3β z-score
MIR17HG positive cells (%)
I
FU/MSI (dMMR)
IC50
R = 0.5069
P = 0.0451
KDM4C
J
MIR17HG&KDM4C
low group
high group
Survival probability (%)
P = 0.024
Time (Months)

Table 1 Clinic-pathological characteristics of 5-FU-treated CRC patients.

No.	Sex	Age	Stage	Tumor size	Recurrence site	Differentiation
1	Male	82	pT3N1M1	4.5 cm × 3.0 cm	Liver	G2
2	Male	79	pT3N1cMx	3.5 cm × 5.0 cm	Small intestine	G2-G3
3	Female	73	T3N2bM1a	5.0 cm × 4.8 cm	Liver	G2
4	Male	56	pT4bN0M1	5.0 cm × 4.5 cm	Lymph nodes	G1−G2
5	Male	51	pT3N2bMx	3.0 cm × 3.0 cm	Lymph nodes	G3
6	Male	74	pT3N1bMx	3.0 cm × 2.0 cm	Lymph nodes	G1−G2
7	Female	76	pT3N2aMx	5.0 cm × 4.0 cm	Lymph nodes	G2−G3
8	Female	60	pT4bN0M1	4.2 cm × 3.5 cm	Liver	G2−G3
9	Female	61	pT3N1aMx	5.5 cm × 4.0 cm	Lymph nodes	G2−G3
10	Female	67	pT3N1cMx	9.0 cm × 8.0 cm	Lymph nodes	G2−G3
11	Female	79	pT3N1bMx	5.5 cm × 4.0 cm	Lymph nodes	G2−G3
12	Male	56	pT3N1cMx	4.5 cm × 4.5 cm	Small intestine	G2−G3
13	Female	63	pT3N2aMx	2.7 cm × 2.0 cm	Lymph nodes	G2
14	Female	78	pT3N1aMx	6.5 cm × 4.5 cm	Lymph nodes	G2
15	Female	61	pT4bN0M1	4.2 cm × 1.5 cm	Lymph nodes	G2−G3
16	Female	68	pT3N1bMx	5.5 cm × 3.5 cm	Lymph nodes	G2
17	Male	68	pT3N1bMx	3.5 cm × 3.5 cm	Lymph nodes	G2
18	Male	73	pT3N1bMx	5.0 cm × 4.0 cm	No recurrence	G2−G3
19	Male	35	pT4N0Mx	10.0 cm × 10.0 cm	No recurrence	G2
20	Male	65	pT2N0Mx	4.0 cm × 3.0 cm	No recurrence	G2
21	Female	72	pT3N0Mx	7.5 cm × 6.0 cm	No recurrence	G2
22	Male	46	pT3N0Mx	4.0 cm × 2.5 cm	No recurrence	G2−G3
23	Male	65	pT3N0Mx	3.5 cm × 2.5 cm	No recurrence	G2
24	Male	71	pT2N0Mx	4.0 cm × 3.0 cm	No recurrence	G2
25	Female	23	pT3N0Mx	6.0 cm × 4.0 cm	No recurrence	G2
26	Female	63	pT3N0Mx	4.0 cm × 2.0 cm	No recurrence	G2
27	Female	73	pT4N1cM1	6.0 cm × 4.5 cm	No recurrence	G2
28	Male	73	pT4N0Mx	5.0 cm × 4.0 cm	No recurrence	G2
29	Male	55	pT3N0Mx	5.0 cm × 3.0 cm	No recurrence	G2
30	Male	64	pT3N0Mx	4.5 cm × 1.3 cm	No recurrence	G2
31	Female	51	pT3N0Mx	6.0 cm × 1.5 cm	No recurrence	G2

The discovery of novel biomarkers predicting response to cancer chemotherapy could aid in patient stratification and enable more effective use of existing chemotherapy and avoid unnecessary toxicity for those patients who would not benefit[46]. Clinical samples grouped as "5-FU-sensitive" or "5-FU resistant" patients were analyzed and found that resistant patients had significantly higher expression of KDM4C and *MIR17HG* and lower expression of Bim and GSK-3β (Fig. 9B and C). Consistently, correlation analysis indicated that *MIR17HG* and KDM4C expression were positively correlated, and *MIR17HG* was inversely correlated with Bim and GSK-3β expression (Fig. 9F−H). Our findings support that the KDM4C/*MIR17HG*/GSK-3β negative feedback loop can serve as a predictive marker for 5-FU response and as a promising therapeutic target for CRC chemoresistance. Expanded clinical samples are needed to further validate the predictive and therapeutic role of the KDM4C/*MIR17HG*/GSK-3β negative feedback loop in CRC chemotherapy response. Additionally, a primary cause of chemotherapy failure in CRC is the inevitable toxic side effects such as gastrointestinal toxicity, immunosuppression, and liver and kidney damage[27], thus explaining the importance of combinational therapy of front-line drug and novel natural compounds in tumor treatment, which may achieve better outcome and limit adverse effects. The present study systematically evaluated the safety of the combination of AVN A and 5-FU *in vivo*.

Together, there are two benefits of combination therapy of 5-FU and AVN A. Firstly, the dose of 5-FU in co-treatment was much lower than that of 5-FU alone in inducing cancer cell death, thereby alleviating the 5-FU-related toxicity. Secondly, AVN A plays a key role in ameliorating immunosuppression and organ damage. The aforementioned advantages are critical in determining the optimal treatment regimen and point out that 5-FU and AVN A in combination as a promising candidate for CRC clinical trials.

Figure 9 The KDM4C/*MIR17HG*/Bim signaling axis is identified as a predictor of 5-FU response. (A) Schematic representation of primary tumor specimens and recurrent or metastatic specimens collected from the same patient who received 5-FU-based therapy. (B) Representative FISH images of *MIR17HG* and corresponding IHC images of KDM4C, GSK-3β, and Bim in 5-FU-based CRC specimens. Scale bars, 50 μm (main) and 500 μm (inset). (C−E) Z-scores of Bim (C), KDM4C (D), and GSK-3β (E) in CRC tissues were analyzed. 5-FU sensitive group, $n = 14$; 5-FU resistant group, $n = 17$. (F−H) Scatter plots showing the correlations between *MIR17HG* and Bim expression (F), *MIR17HG* and KDM4C expression (G), and *MIR17HG* and GSK-3β expression (H) in CRC samples, respectively. $n = 31$. (I) The correlation of 5-FU sensitivity and KDM4C levels in MSI CRC cell lines was analyzed by the GDSC dataset. (J) Kaplan−Meier survival analysis shows the overall survival of CRC patients with indicated tumor genotype in TCGA. $^{*}P < 0.05$; $^{**}P < 0.01$; $^{***}P < 0.001$.

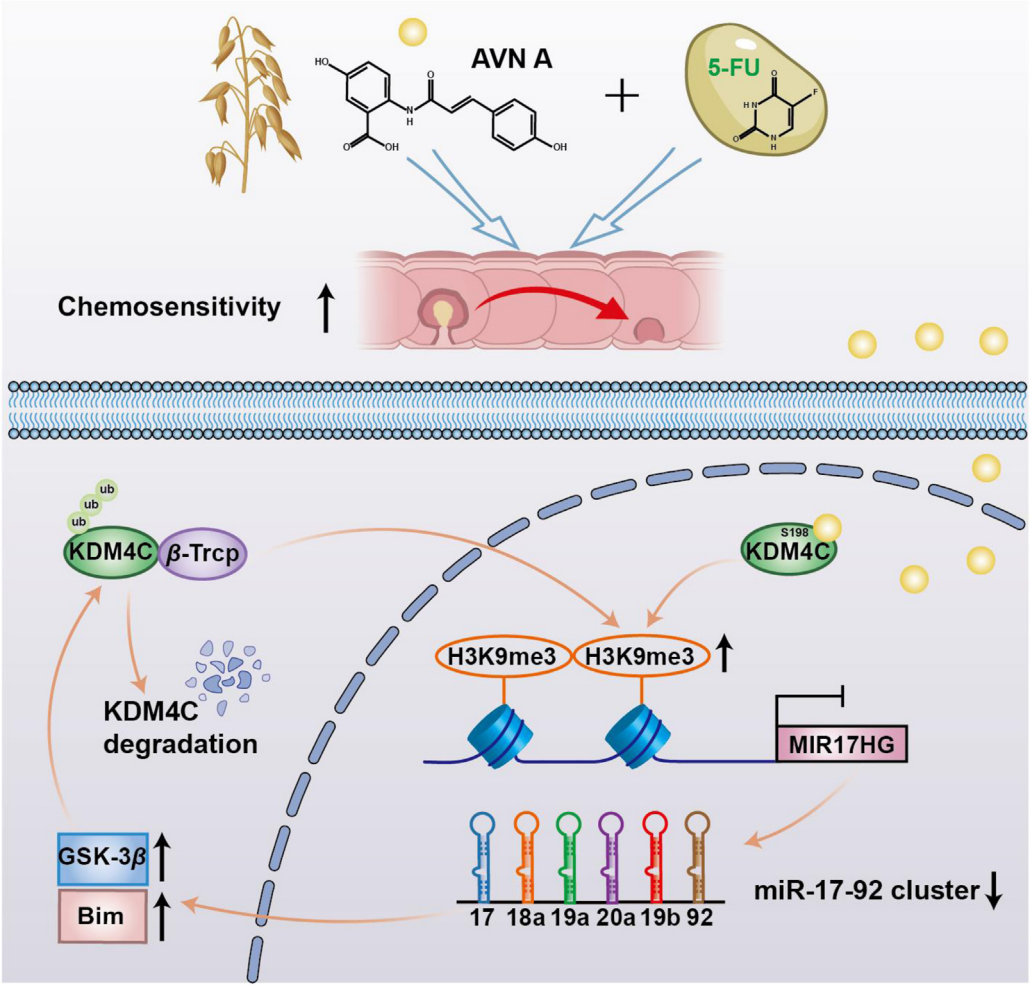

Figure 10 A schematic illustration of the proposed mechanism of AVN A sensitizes CRC to chemotherapeutic response.

5. Conclusions

Our findings highlight that AVN A combined with 5-FU confers a remarkable synergetic and selective anti-tumor activity in CRC cells and xenograft models. The KDM4C/*MIR17HG*/Bim axis is shown to be critical for AVN A-potentiated therapeutic response based on clinical samples, TCGA database, and functional experiments. AVN A directly binds to the S198 residue of KDM4C to block *MIR17HG* transcription, thus driving CRC cells toward a proapoptotic state and making CRC cells more vulnerable to 5-FU. AVN A improved the therapeutic efficacy of 5-FU *via* impairing the KDM4C/*MIR17HG*/GSK-3β negative feedback loop. Our data identified KDM4C/*MIR17HG*/GSK-3β negative feedback loop as a predictor of therapy response and vulnerability and proposed a novel treatment option that AVN A could be a promising adjuvant for 5-FU-centric therapy on CRC.

Acknowledgments

This work was supported by the National Natural Science Foundation of China (Nos. 32200321, 82270217, 31800657, and 32072220), National Natural Science Foundation of China Regional Innovation and Development Joint Fund Key Support Project (U23A20526, China), Natural Science Foundation of Shanxi Province (Nos. 20210302124252, and 202203021211293, China), Scientific and Technological Innovation Programs of Higher Education Institutions in Shanxi (2021L212, China), and "1331 Project" Key Innovation Team of Shanxi Province (Prof. Zhuoyu Li).

Author contributions

Rong Fu: Conceptualization, Data curation, Funding acquisition, Writing – original draft. Zhangfeng Dou: Formal analysis, Software. Ning Li: Data curation, Investigation. Xueyuan Fan: Data curation, Formal analysis, Investigation. Sajid Amin: Investigation, Writing – review & editing. Jinqi Zhang: Data curation, Formal analysis. Yuqing Wang: Data curation, Formal analysis, Methodology. Zongwei Li: Data curation, Funding acquisition, Writing – review & editing. Zhuoyu Li: Funding acquisition, Writing – review & editing. Peng Yang: Conceptualization, Funding acquisition, Writing – review & editing.

Conflicts of interest

The authors declare that there is no conflict of interest.

Appendix A. Supporting information

Supporting information to this article can be found online at https://doi.org/10.1016/j.apsb.2024.07.018.

References

1. Bray F, Ferlay J, Soerjomataram I, Siegel RL, Torre LA, Jemal A. Global cancer statistics 2018: GLOBOCAN estimates of incidence and mortality worldwide for 36 cancers in 185 countries. *CA Cancer J Clin* 2018;**68**:394−424.
2. Keum N, Giovannucci E. Global burden of colorectal cancer: emerging trends, risk factors and prevention strategies. *Nat Rev Gastroenterol Hepatol* 2019;**16**:713−32.
3. Rich TA, Shepard RC, Mosley ST. Four decades of continuing innovation with fluorouracil: current and future approaches to fluorouracil chemoradiation therapy. *J Clin Oncol* 2004;**22**:2214−32.
4. Combes E, Andrade AF. Inhibition of ataxia-telangiectasia mutated and rad3-related (ATR) overcomes oxaliplatin resistance and promotes antitumor immunity in colorectal cancer. *Cancer Res* 2019;**79**: 2933−46.
5. Azwar S, Seow HF, Abdullah M, Faisal Jabar M, Mohtarrudin N. Recent updates on mechanisms of resistance to 5-fluorouracil and reversal strategies in colon cancer treatment. *Biology* 2021;**10**: 854.
6. Blondy S, David V. 5-Fluorouracil resistance mechanisms in colorectal cancer: from classical pathways to promising processes. *Cancer Sci* 2020;**111**:3142−54.
7. Walsh J, Haddock J, Blumberg JB, McKay DL, Wei X, Dolnikowski G, et al. Identification of methylated metabolites of oat avenanthramides in human plasma using UHPLC QToF-MS. *Int J Food Sci Nutr* 2018;**69**:377−83.
8. Fu R, Yang P, Sajid A, Li Z. Avenanthramide A induces cellular senescence *via* miR-129-3p/Pirh2/p53 signaling pathway to suppress colon cancer growth. *J Agric Food Chem* 2019;**67**:4808−16.
9. Fu R, Yang P, Li Z, Liu W, Amin S, Li Z. Avenanthramide A triggers potent ROS-mediated anti-tumor effects in colorectal cancer by directly targeting DDX3. *Cell Death Dis* 2019;**10**:593.
10. Mogilyansky E, Rigoutsos I. The miR-17/92 cluster: a comprehensive update on its genomics, genetics, functions and increasingly important and numerous roles in health and disease. *Cell Death Differ* 2013;**20**: 1603−14.
11. Morelli E, Biamonte L, Federico C, Amodio N, Di Martino MT, Gallo Cantafio ME, et al. Therapeutic vulnerability of multiple myeloma to MIR17PTi, a first-in-class inhibitor of pri-miR-17-92. *Blood* 2018; **132**:1050−63.
12. Xiao C, Srinivasan L, Calado DP, Patterson HC, Zhang B, Wang J, et al. Lymphoproliferative disease and autoimmunity in mice with increased miR-17-92 expression in lymphocytes. *Nat Immunol* 2008;**9**: 405−14.
13. Hu T, Chong Y, Qin H, Kitamura E, Chang CS, Silva J, et al. The miR-17/92 cluster is involved in the molecular etiology of the SCLL syndrome driven by the BCR-FGFR1 chimeric kinase. *Oncogene* 2018; **37**:1926−38.
14. Qiu H, Liu N, Luo L, Zhong J, Tang Z, Kang K, et al. MicroRNA-17-92 regulates myoblast proliferation and differentiation by targeting the ENH1/Id1 signaling axis. *Cel Death Differ* 2016;**23**:1658−69.
15. Awan FM, Naz A, Obaid A, Ikram A, Ali A, Ahmad J, et al. MicroRNA pharmacogenomics based integrated model of miR-17-92 cluster in sorafenib resistant HCC cells reveals a strategy to forestall drug resistance. *Sci Rep* 2017;**7**:11448.
16. Yang H, Lan P, Hou Z, Guan Y, Zhang J, Xu W, et al. Histone deacetylase inhibitor SAHA epigenetically regulates miR-17-92 cluster and MCM7 to upregulate MICA expression in hepatoma. *Br J Cancer* 2015;**112**:112−21.
17. Sun Y, Li S, Yu W, Zhao Z, Gao J, Chen C, et al. *N*(6)-Methyladenosine-dependent pri-miR-17-92 maturation suppresses PTEN/TMEM127 and promotes sensitivity to everolimus in gastric cancer. *Cel Death Dis* 2020;**11**:836.
18. Zhao E, Ding J, Xia Y, Liu M, Ye B, Choi JH, et al. KDM4C and ATF4 cooperate in transcriptional control of amino acid metabolism. *Cell Rep* 2016;**14**:506−19.
19. Mikkelsen TS, Ku M, Jaffe DB, Issac B, Lieberman E, Giannoukos G, et al. Genome-wide maps of chromatin state in pluripotent and lineage-committed cells. *Nature* 2007;**448**:553−60.
20. Yu Y, Schleich K, Yue B, Ji S, Lohneis P, Kemper K, et al. Targeting the senescence-overriding cooperative activity of structurally unrelated H3K9 demethylases in melanoma. *Cancer Cell* 2018;**33**: 322−36.
21. Chen Y, Fang R, Yue C, Chang G, Li P, Guo Q, et al. Wnt-induced stabilization of KDM4C is required for Wnt/β-Catenin target gene expression and glioblastoma tumorigenesis. *Cancer Res* 2020;**80**: 1049−63.
22. Xue X, Yang YA, Zhang A, Fong KW, Kim J, Song B, et al. LncRNA HOTAIR enhances ER signaling and confers tamoxifen resistance in breast cancer. *Oncogene* 2016;**35**:2746−55.
23. Qu Y, Olsen JR, Yuan X, Cheng PF, Levesque MP, Brokstad KA. Small molecule promotes β-catenin citrullination and inhibits Wnt signaling in cancer. *Nat Chem Biol* 2018;**14**:94−101.
24. Yang P, Ding GB, Liu W, Fu R, Sajid A, Li Z. Tannic acid directly targets pyruvate kinase isoenzyme M2 to attenuate colon cancer cell proliferation. *Food Funct* 2018;**9**:5547−59.
25. Zheng CC, Liao L, Liu YP, Yang YM, He Y, Zhang GG, et al. Blockade of nuclear β-Catenin signaling *via* direct targeting of RanBP3 with NU2058 induces cell senescence to suppress colorectal tumorigenesis. *Adv Sci* 2022;**9**:e2202528.
26. Ashton JC. Drug combination studies and their synergy quantification using the Chou-Talalay method—letter. *Cancer Res* 2015;**75**: 2400.
27. Goirand F, Lemaitre F, Launay M, Tron C, Chatelut E, Boyer JC, et al. How can we best monitor 5-FU administration to maximize benefit to risk ratio?. *Expert Opin Drug Metab Toxicol* 2018;**14**: 1303−13.
28. Ashkenazi A, Fairbrother WJ, Leverson JD, Souers AJ. From basic apoptosis discoveries to advanced selective BCL-2 family inhibitors. *Nat Rev Drug Discov* 2017;**16**:273−84.
29. Weng H, Huang H, Dong B, Zhao P, Zhou H, Qu L. Inhibition of miR-17 and miR-20a by oridonin triggers apoptosis and reverses chemoresistance by derepressing BIM-S. *Cancer Res* 2014;**74**:4409−19.
30. Monroig Pdel C, Chen L, Zhang S, Calin GA. Small molecule compounds targeting miRNAs for cancer therapy. *Adv Drug Deliv Rev* 2015;**81**:104−16.
31. Cheung N, Fung TK, Zeisig BB, Holmes K, Rane JK, Mowen KA, et al. Targeting aberrant epigenetic networks mediated by PRMT1 and KDM4C in acute myeloid leukemia. *Cancer Cell* 2016;**29**: 32−48.
32. Jie X, Fong WP, Zhou R, Zhao Y, Zhao Y, Meng R, et al. USP9X-mediated KDM4C deubiquitination promotes lung cancer radioresistance by epigenetically inducing TGF-β2 transcription. *Cel Death Differ* 2021;**28**:2095−111.
33. Ibrahim SSA, Kandil LS, Ragab GM, El-Sayyad SM. Micro RNAs 26b, 20a inversely correlate with GSK-3β/NF-κB/NLRP-3 pathway to highlight the additive promising effects of atorvastatin and quercetin in experimental induced arthritis. *Int Immunopharmacol* 2021;**99**: 108042.
34. Yu FB, Sheng J, Yu JM, Liu JH, Qin XX, Mou B. MiR-19a-3p regulates the Forkhead box F2-mediated Wnt/β-catenin signaling pathway and affects the biological functions of colorectal cancer cells. *World J Gastroenterol* 2020;**26**:627−44.
35. Ou J, Peng Y, Yang W, Zhang Y, Hao J, Li F, et al. ABHD5 blunts the sensitivity of colorectal cancer to fluorouracil *via* promoting autophagic uracil yield. *Nat Commun* 2019;**10**:1078.
36. Aune D, Keum N, Giovannucci E, Fadnes LT, Boffetta P, Greenwood DC, et al. Whole grain consumption and risk of cardiovascular disease, cancer, and all cause and cause specific mortality: systematic review and dose-response meta-analysis of prospective studies. *BMJ* 2016;**353**:i2716.
37. Wang W, Snooks HD, Sang S. The chemistry and health benefits of dietary phenolamides. *J Agric Food Chem* 2020;**68**:6248−67.

38. Tanaka K, Yu HA, Yang S, Han S, Selcuklu SD, Kim K, et al. Targeting Aurora B kinase prevents and overcomes resistance to EGFR inhibitors in lung cancer by enhancing BIM- and PUMA-mediated apoptosis. *Cancer Cell* 2021;**39**:1245−61.
39. Khatoon E, Banik K, Harsha C, Sailo BL, Thakur KK, Khwairakpam AD, et al. Phytochemicals in cancer cell chemosensitization: current knowledge and future perspectives. *Semin Cancer Biol* 2022;**80**:306−39.
40. Mastropasqua F, Marzano F, Valletti A, Aiello I, Di Tullio G, Morgano A, et al. TRIM8 restores p53 tumour suppressor function by blunting N-MYC activity in chemo-resistant tumours. *Mol Cancer* 2017;**16**:67.
41. Han YC, Vidigal JA, Mu P, Yao E, Singh I, Gonzalez AJ, et al. An allelic series of miR-17 approximately 92-mutant mice uncovers functional specialization and cooperation among members of a microRNA polycistron. *Nat Genet* 2015;**47**:766−75.
42. Izreig S, Samborska B, Johnson RM, Sergushichev A, Ma EH, Lussier C, et al. The miR-17∼92 microRNA cluster is a global regulator of tumor metabolism. *Cel Rep* 2016;**16**:1915−28.
43. Lee YH, Song NY, Suh J, Kim DH, Kim W, Ann J, et al. Curcumin suppresses oncogenicity of human colon cancer cells by covalently modifying the cysteine 67 residue of SIRT1. *Cancer Lett* 2018;**431**:219−29.
44. Hegde NS, Sanders DA, Rodriguez R, Balasubramanian S. The transcription factor FOXM1 is a cellular target of the natural product thiostrepton. *Nat Chem* 2011;**3**:725−31.
45. Elgendy M, Cirò M, Hosseini A, Weiszmann J, Mazzarella L, Ferrari E, et al. Combination of hypoglycemia and metformin impairs tumor metabolic plasticity and growth by modulating the PP2A−GSK3β−MCL-1 Axis. *Cancer Cell* 2019;**35**:798−815.
46. Jin L, Chun J, Pan C, Li D, Lin R, Alesi GN, et al. MAST1 drives cisplatin resistance in human cancers by rewiring cRaf-independent MEK activation. *Cancer Cell* 2018;**34**:315−30.